1   **The universal suppressor mutation in the HSV-1 nuclear egress complex restores**

2   **membrane budding defects by stabilizing the oligomeric lattice.**

3

4   Elizabeth B. Draganova[1,†], Hui Wang[2,3,4], Melanie Wu[5], Shiqing Liao[2,4], Amber Vu[6], Gonzalo L.

5   Gonzalez-Del Pino[1], Z. Hong Zhou[2,3,4], Richard J. Roller[6], and Ekaterina E. Heldwein[1,*]

6

7   [1]Department of Molecular Biology and Microbiology, Tufts University School of Medicine,

8   Boston, MA, USA

9   [2]Department of Microbiology, Immunology & Molecular Genetics, University of California, Los

10   Angeles (UCLA), Los Angeles, CA, USA

11   [3]Department of Bioengineering, UCLA, Los Angeles, CA, USA

12   [4]California NanoSystems Institute, UCLA, Los Angeles, United States

13   [5]School of Chemistry and Molecular Biosciences, The University of Queensland, Brisbane,

14   Australia

15   [6]Department of Microbiology and Immunology, Carver College of Medicine, University of Iowa,

16   Iowa City, IA, USA

17   [†]Current address: Department of Biochemistry, Emory University School of Medicine, Atlanta,

18   GA, USA

19

20   *Correspondence:

21   Ekaterina E. Heldwein

22   Phone: (617) 636-0858

23   Fax: (617) 636-0337

24   katya.heldwein@tufts.edu

25

26   Short title: Larger oligomeric interfaces restore membrane budding defects in HSV-1 NEC.

27

28   Keywords: herpes simplex virus, nuclear egress, nuclear egress complex, budding,

29   oligomerization, lattice, suppression

30

31   **ABSTRACT**

32   Nuclear egress is an essential process in herpesviral replication whereby nascent capsids

33   translocate from the nucleus to the cytoplasm. This initial step of nuclear egress – budding at the

34   inner nuclear membrane – is coordinated by the nuclear egress complex (NEC). Composed of the

35   viral proteins UL31 and UL34, NEC deforms the membrane around the capsid as the latter buds

36   into the perinuclear space. NEC oligomerization into a hexagonal membrane-bound lattice is

37   essential for budding because mutations designed to perturb lattice interfaces reduce its budding

38   ability. Previously, we identified an NEC suppressor mutation capable of restoring budding to a

39   mutant with a weakened hexagonal lattice. Here, we show that the suppressor mutation can

40   restore budding to a broad range of budding-deficient NEC mutants thereby acting as a universal

41   suppressor. We demonstrate that the suppressor mutation indirectly promotes the formation of

42   new contacts between the NEC hexamers that, ostensibly, stabilize the hexagonal lattice. This

43   stabilization strategy is powerful enough to override the otherwise deleterious effects of

44   mutations that destabilize the NEC lattice by different mechanisms, resulting in a functional

45   NEC hexagonal lattice and restoration of membrane budding.

46

INTRODUCTION

Viruses are experts at reorganizing host membranes to traffic their capsids across the compartmentalized interior of eukaryotic cells. One of the more unusual mechanisms of membrane manipulation is found in *Herpesvirales*, which is an order of large, enveloped viruses that infect multiple species across the animal kingdom and cause life-long infections in the majority of the world's population. Replication of herpesviral dsDNA genomes and their subsequent packaging into capsids occurs within the nucleus. Genome-containing capsids are then transported into the cytoplasm for maturation into infectious virions. Most of the nucleocytoplasmic traffic occurs through the nuclear pores, but at ~125 nm in diameter, herpesviral capsids are too large to fit through the ~40-nm nuclear pore opening. Instead, the capsids use a complex, non-canonical nuclear transport route termed nuclear egress [1-3]. First, they dock at the inner nuclear membrane (INM) and bud into the perinuclear space, producing perinuclear enveloped virions (a stage termed primary envelopment). The envelopes of these intermediates then fuse with the outer nuclear membrane (ONM) and capsids are then released into the cytoplasm (a stage termed de-envelopment).

The nuclear egress mechanism is best understood for the family *Herpesviridae*, commonly referred to as herpesviruses, which infect mammals, birds, and reptiles. Two conserved viral proteins, called UL31 and UL34 in herpes simplex virus (HSV), are essential for nuclear egress in herpesviruses. UL31 is a soluble nuclear phosphoprotein [4,5] whereas UL34 is a type I membrane protein containing a single C-terminal transmembrane helix [4,6]. Together, UL31 and UL34 form the heterodimeric nuclear egress complex (NEC) that is anchored in the INM and faces the nuclear interior. Both proteins are essential for nuclear egress, and in the absence of either, capsids become trapped within the nucleus, which results in greatly reduced viral titers [4,5,7-11]. Moreover, overexpression of both UL31 and UL34 in uninfected cells causes the accumulation of empty budded vesicles in the perinuclear space, which implies that the NEC is not only necessary but also sufficient for the INM budding [12-16]. Collectively, these findings highlight the central role of the NEC during nuclear egress.

Recent studies with purified recombinant NEC and synthetic lipid vesicles have shown that several NEC homologs can deform and bud membranes *in vitro* in the absence of added energy or other proteins. These include the NECs from herpes simplex virus 1 (HSV-1) [17], a prototypical herpesvirus that infects much of the world's population; the closely related

78   pseudorabies virus (PRV) that infects animals [18]; and the more distantly related Epstein-Barr

79   Virus (EBV) [19], a nearly ubiquitous human herpesvirus.

80   The NEC oligomerizes into membrane-bound coats on the inner surface of the budded

81   vesicles. Hexagonal coats resembling a honeycomb have been observed by cryo-electron

82   microscopy/tomography (cryo-EM/ET) on vesicles formed by recombinant HSV-1 NEC *in vitro*

83   [17], vesicles formed in uninfected cells overexpressing PRV NEC [20], and in perinuclear vesicles

84   formed in HSV-1-infected cells [21]. Interestingly, crystallized NEC homologs from HSV-1 [22] and

85   human cytomegalovirus (HCMV) [23] also formed hexagonal crystal lattices of geometry and

86   dimensions similar to those observed in the membrane-bound NEC coats. Finally, EBV NEC

87   also forms membrane-bound coats *in vitro* but their geometry is yet unclear [19]. Both the intrinsic

88   membrane budding ability and the formation of oligomeric coats thus appear to be conserved

89   among the NEC homologs.

90   In HSV-1 NEC, oligomerization into the hexagonal lattice is essential for budding.

91   Mutations targeting lattice interfaces within the NEC hexamers (hexameric) or between

92   hexamers (interhexameric) cause budding defects *in vitro* [17,22] and reduce nuclear egress in

93   infected cells [24,25]. The first such mutation, $D35A_{UL34}/E37A_{UL34}$, was identified in a mutational

94   screen targeting charge clusters in the HSV-1 UL34 sequence [26]. This double mutation reduced

95   viral titers by ~3 orders of magnitude to levels of UL34-null mutant HSV-1 and blocked capsid

96   egress from the nucleus in a dominant-negative manner [25]. Therefore, we refer to it as DN_{UL34}.

97   The mutation did not affect the NEC formation, its localization to the INM, or capsid docking at

98   the INM but, instead, precluded capsid budding [25]. Furthermore, purified recombinant NEC-

99   DN_{UL34} bound synthetic membranes *in vitro* but had minimal membrane-budding activity and did

100   not form hexagonal coats on membranes [17].

101   Interestingly, the nuclear budding defect due to the DN_{UL34} mutation could be suppressed

102   by an extragenic mutation in HSV-1 UL31, $R229L_{UL31}$, which arose during serial passaging of

103   the DN_{UL34} mutant HSV-1 virus on a UL34-complementing cell line [25]. We refer to this mutation

104   as SUP_{UL31}. SUP_{UL31} maps near the interhexameric interface, far away from the DN_{UL34}

105   mutations at hexameric interface [22], making it unclear how the SUP_{UL31} mutation restores DN_{UL34}

106   nuclear budding defects.

107

108   Here, we show that the SUP_{UL31} mutation can restore efficient budding to a broad range

109   of mutants that disrupt important functional interfaces, acting as a "universal" suppressor of

110   budding defects. Using cryo-ET and x-ray crystallography, we show that the SUP_{UL31} mutation

111   does not change the structure of the NEC heterodimer or its oligomerization into hexamers.

112   Instead, it promotes the formation of new contacts at the interhexameric interface. We propose

113   that the increased interhexameric interface reinforces the hexagonal NEC lattice, thereby

114   counteracting the deleterious effects of mutations that perturb it.

115

116   **RESULTS**

117   ***The SUP_{UL31} mutation restores membrane budding in vitro to various oligomeric interface***

118   ***mutants.*** HSV-1 NEC oligomerizes into a hexagonal lattice (**Fig. 1a**) stabilized by interactions

119   between NEC heterodimers within hexamers (hexameric interface; **Fig. 1b**) and between

120   hexamers (interhexameric interface; (**Fig. 1c**). NEC hexameric lattice formation is essential for

121   membrane budding because mutations engineered to disrupt lattice interfaces reduce budding *in*

122   *vitro* [17,22] and nuclear egress in infected cells [24,25]. These budding-deficient mutations are

123    $D35A_{UL34}/E37A_{UL34}$ (DN_{UL34}), $V92F_{UL34}$, $T123Q_{UL34}$, $V247F_{UL31}$, and $F252Y_{UL31}$ at the

124   hexameric interface (**Fig. 1b**) and $E153R_{UL31}$ at the interhexameric interface (**Fig. 1c**). The

125   SUP_{UL31} mutation restores budding *in vitro* to DN_{UL34} and $V92F_{UL34}$ mutants [22]. Here, we asked

126   if it could restore budding to other interface mutants, $T123Q_{UL34}$ and $F252Y_{UL31}$ (hexameric)

127   (**Fig. 1b**) and $E153R_{UL31}$ (interhexameric) (**Fig. 1c**).

128   We also wanted to assess the individual contributions of $D35A_{UL34}$ and $E37A_{UL34}$

129   mutations to the budding-deficient phenotype of the DN_{UL34} mutant. Residue $E37_{UL34}$ is located

130   at the hexameric interface where its side chain forms a hydrogen bond with $T89_{UL31}$ of the

131   neighboring NEC heterodimer. The $E37A_{UL34}$ mutation eliminates this hydrogen bond, which

132   would disrupt the hexameric interface. Indeed, the $E37A_{UL34}$ mutant was deficient in budding *in*

133   *vitro* [22]. However, the side chain of residue $D35_{UL34}$ points away from the hexameric interface

134   (**Fig. 1b**). Therefore, we tested if the $D35A_{UL34}$ mutation would have any effect on budding.
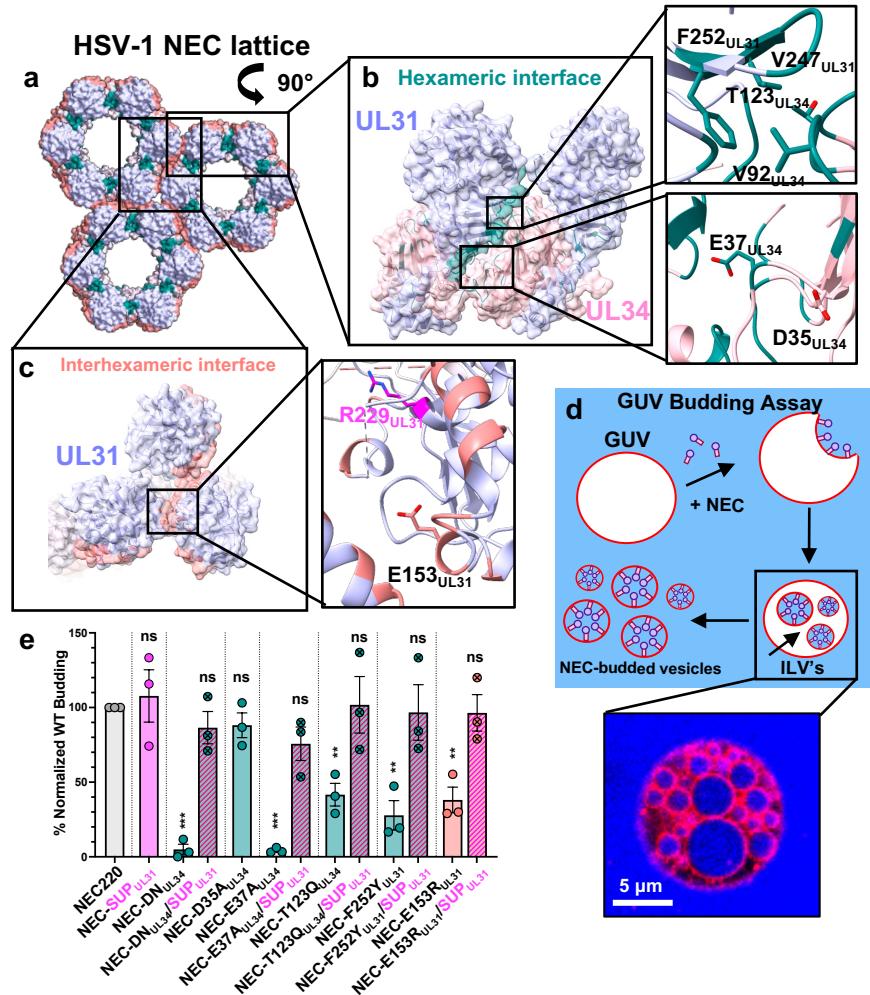
Fig. 1. The SUP$_{UL31}$ mutation restores budding activity to budding-deficient oligomeric interface NEC mutants. a-c) HSV-1 NEC hexameric and interhexameric interfaces highlighting the locations of residues mutated for this study. **d)** A cartoon representation of the GUV budding assay showing the NEC (purple circles and pink rectangles) binding to red fluorescent GUVs and undergoing negative curvature to form an NEC-coated intraluminal vesicle (ILV). Free NEC continues to bud the GUVs until only fully-budded vesicles containing NEC on the interior remain. Cascade blue, a membrane impermeant dye, is used to monitor budding. **e)** SUP-R229L$_{31}$ rescues budding in both hexameric and interhexameric budding-deficient NEC mutants *in vitro*. The percentage of *in vitro* budding was determined by counting the number of ILVs within the GUVs after the addition of NEC220 or the corresponding NEC mutant. A background count, the number of ILVs in the absence of NEC, was subtracted from each condition. Each construct was tested in three biological replicates, each consisting of three technical replicates. Symbols show the average budding efficiency of three technical replicates compared to NEC220 (100%; grey). Significance was calculated using an unpaired Student's t-test with Welch's correction (P < 0.001 = ***; P < 0.0001 = **; ns = not significant) in GraphPad Prism 9.0.

The *in-vitro* budding activity of all NEC mutants was measured by an established assay [17,22,27,28] utilizing fluorescently labeled giant unilamellar vesicles (GUV), soluble fluorescent dye Cascade Blue, and the soluble version of HSV-1 NEC, NEC220, which contained full-length

6

154   UL31 and UL34 residues 1-220 **(Fig. 1d)**. We first confirmed the *in-vitro* phenotypes of the

155   budding-deficient mutants. Both DN_{UL34} and $E37A_{UL34}$ mutations reduced budding to ~10% of

156   the WT NEC220 **(Fig. 1e),** consistent with our previous findings [22] whereas the $D35A_{UL34}$

157   mutation alone had no effect **(Fig. 1e).** Thus, the $E37A_{UL34}$ mutation is solely responsible for the

158   nonbudding phenotype of DN_{UL34}. The interface mutations $T123Q_{UL34}$, $F252Y_{UL31}$, and

159    $E153R_{UL31}$ **(Fig. 1bc)** reduced budding to ~30-40% of the WT NEC220 **(Fig. 1e)**, as previously

160   observed [22]. The SUP_{UL31} mutation did not affect the budding efficiency of the WT NEC220 but

161   restored budding not only to the DN_{UL34} as shown previously [22] but to all other lattice interface

162   mutants regardless of their location **(Fig. 1e)**. Thus, the SUP_{UL31} mutation can restore efficient

163   budding to a broad range of lattice interface mutants.

164

165   ***The SUP_{UL31} mutation complements the growth defects of HSV-1 containing oligomeric***

166   ***interface mutations.*** To correlate the *in-vitro* budding phenotypes with the infected cell

167   phenotypes, we used an established viral growth complementation assay [9]. This assay measures

168   the ability of a mutant protein expressed *in trans* to complement the poor growth of a virus

169   lacking the corresponding gene (the so-called null virus). Hep-2 cells were transfected with

170   plasmids encoding either WT, mutant UL34 ($D35A_{UL34}/E37A_{UL34}$, $D35A_{UL34}$, $E37A_{UL34}$,

171    $T123Q_{UL34}$), or mutant UL31 ($F252Y_{UL31}$ and $E153R_{UL31}$) and then infected with either a UL34-

172   null HSV-1 or UL31-null HSV-1. The amount of infectious viral progeny produced was

173   measured by plaque assay on either UL34-expressing **(Fig. 2a)** or UL31-expressing Vero cells

174   **(Fig. 2b).** We found that cells expressing the $D35A_{UL34}/E37A_{UL34}$, $E37A_{UL34}$, $T123Q_{UL34}$, or

175    $E153R_{UL31}$ mutants poorly complemented replication of either the UL34-null **(Fig. 2a)** or UL31-

176   null HSV-1 **(Fig. 2b)**, respectively, *in trans***,** in agreement with their impaired budding

177   phenotypes *in vitro*. By contrast, the $D35A_{UL34}$ mutant complemented UL34-null HSV-1 *in trans*

178   with an efficiency similar to that of the WT UL34 **(Fig. 2a)**. Surprisingly, the $F252Y_{UL31}$ mutant

179   complemented UL31-null HSV-1 *in trans* similarly to WT UL31 despite reduced budding

180   efficiency in our *in-vitro* budding assay **(Fig. 1e)**.

181   To rule out increased protein expression levels as the *in-trans* complementation

182   mechanism, we measured expression levels of transfected WT UL34, WT UL31, and the

183   corresponding mutant proteins during infection with the corresponding null virus. All mutant

184   UL34 proteins expressed at levels similar to that of WT UL34 **(Fig. S1)**. Reduced

7

185   complementation efficiencies of D35A$_{UL34}$/E37A$_{UL34}$, E37A$_{UL34}$, and T123Q$_{UL34}$ (**Fig. 2a**) are

186   thus due to the specific mutation(s). In contrast, both F252Y$_{UL31}$ and E153R$_{UL31}$ are

187   overexpressed relative to the WT UL31 and R229L$_{UL31}$. Efficient complementation by the

188   F252Y$_{UL31}$ mutant is likely due to its higher expression levels (**Fig. 2b**).
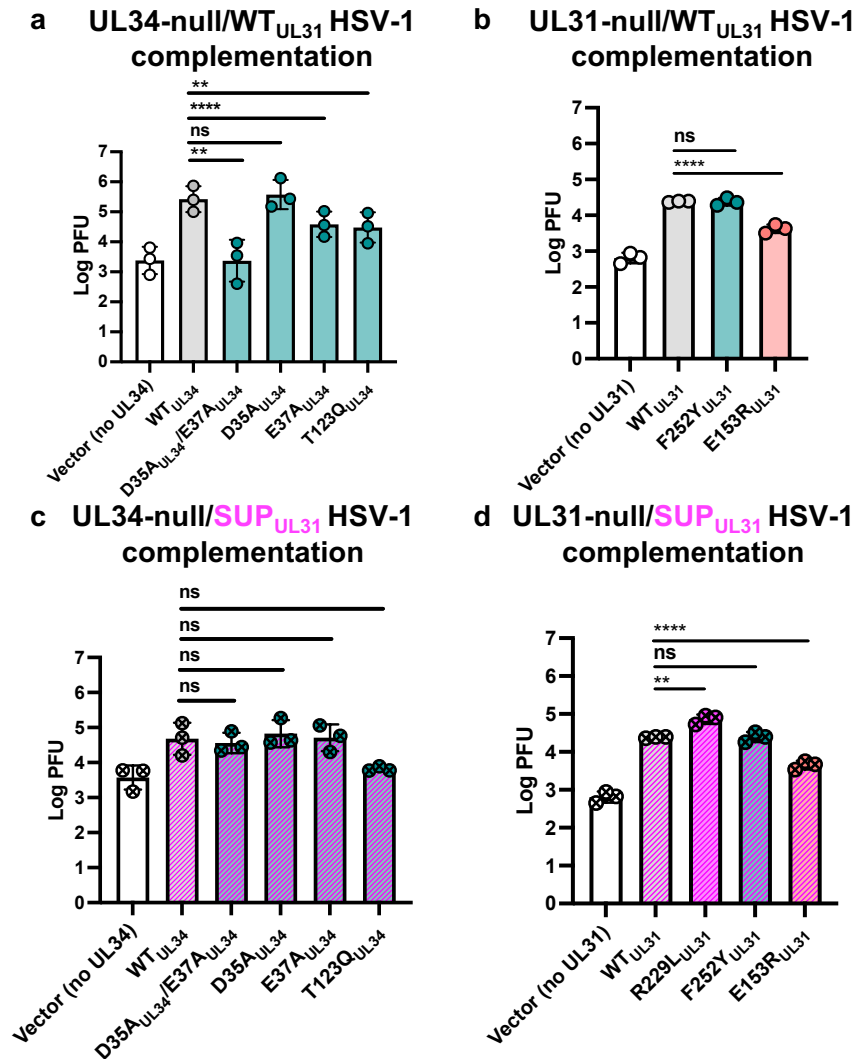
189

190   **Fig. 2. The SUP$_{UL31}$ mutation complements the growth defects of HSV-1 containing oligomeric interface**
191   **mutations. (a-b)** WT$_{UL31}$ can only complement the growth of the D35A$_{UL34}$ and F252Y$_{UL31}$ oligomeric
192   interface mutants whereas SUP$_{UL31}$ can complement more **(c-d)**. For all experiments, Hep-2 cells were
193   transfected with the corresponding UL34 or UL31 mutant plasmid and infected with either a UL34-
194   null/UL31$_{WT}$ virus **(a),** a UL31-null/UL31$_{WT}$ virus **(b)**, a UL34-null/UL31$_{R229L}$ virus **(c)**, or a UL31-
195   null/UL31$_{R229L}$ virus **(d)**. Each bar represents the mean of three independent experiments. Statistical
196   significance was determined by performing a paired two-tailed t-test of each mutant against the WT in
197   GraphPad Prism. P < 0.01 = **; P < 0.0001 = ****; ns, not significant.

198

199   To probe the ability of the SUP$_{UL31}$ mutation to restore efficient complementation to the

200   UL34 and UL31 mutants, i.e., to suppress their complementation defects, we generated the

8

201   UL34-null/SUP$_{UL31}$ and UL31-null/SUP$_{UL31}$ mutant HSV-1 viruses. Hep-2 cells were transfected

202   with plasmids encoding either WT UL34, mutant UL34 (D35A$_{UL34}$/E37A$_{UL34}$, D35A$_{UL34}$,

203   E37A$_{UL34}$, T123Q$_{UL34}$), WT UL31, or mutant UL31 (F252Y$_{UL31}$ and E153R$_{UL31}$), and then

204   infected with either a UL34-null/SUP$_{UL31}$ or UL31-null/SUP$_{UL31}$ HSV-1 (instead of a UL34-null

205   or UL31-null HSV-1). HSV-1 containing the SUP$_{UL31}$ mutation replicates less efficiently than

206   the WT HSV-1, yielding ~1-log-fold lower viral titer **(Fig. 2cd),** as reported previously [25].

207   Therefore, complementation of either the UL34-null/SUP$_{UL31}$ or UL31-null/SUP$_{UL31}$ viruses by

208   the WT UL34 or UL31, respectively, was used as a reference point for assessing the ability of

209   the SUP$_{UL31}$ mutation to restore efficient complementation to UL34 and UL31 mutants. Indeed,

210   the SUP$_{UL31}$ mutation suppressed the complementation defects of both the D35A$_{UL34}$/E37A$_{UL34}$

211   and E37A$_{UL34}$ mutants similarly to the WT UL34 **(Fig. 2c).** Unsurprisingly, the SUP$_{UL31}$

212   mutation had no obvious effect on the already efficient complementation by the D35A$_{UL34}$ **(Fig.**

213   **2c)** and F252Y$_{UL31}$ mutants **(Fig. 2d).** However, it was unable to fully restore the poor

214   complementation by either the T123Q$_{UL34}$ **(Fig. 2c)** or E153R$_{UL31}$ mutants **(Fig. 2d)** despite

215   restoring their budding defects *in vitro.* We hypothesize that the T123Q$_{UL34}$ and E153R$_{UL31}$

216   mutations may impair some other important viral replication function of UL34 or UL31,

217   respectively, that cannot be suppressed by the SUP$_{UL31}$ mutation, e.g., nuclear lamina dissolution,

218   capsid docking at the INM, or capsid recruitment.

219

220   ***The SUP$_{UL31}$ mutation restores efficient budding in vitro to heterodimeric interface mutants***

221   ***and complements their viral growth defects.*** The aforementioned mutational screen targeting

222   charge clusters in the HSV-1 UL34 sequence [26], identified another double mutant,

223   K137A$_{UL34}$/R139A$_{UL34}$, that could not trans-complement the growth of the HSV-1 UL34-null

224   virus. This suggested that residues K137$_{UL34}$ and R139$_{UL34}$ are important for HSV-1 replication.

225   The double mutation did not affect the NEC localization to the INM, suggesting a defect in the

226   NEC function [26]. In the HSV-1 NEC crystal structure, K137$_{UL34}$ forms salt bridges with E67$_{UL34}$

227   and Y61$_{UL31}$ at the heterodimeric interface between the globular domains of UL31 and UL34

228   **(Fig. 3a, inset)**. Thus, K137$_{UL34}$ could contribute to the stabilization of the NEC heterodimer. By

229   contrast, R139$_{UL34}$ does not form any obvious interactions **(Fig. 3a, inset)**.

230   To test the effect of the K137A$_{UL34}$, R139A$_{UL34}$, and K137A$_{UL34}$/R139A$_{UL34}$ mutations on

231   the heterodimer stability and budding activity *in vitro*, we introduced them into the recombinant

9

232   NEC220. Typically, size-exclusion chromatography on samples of purified, WT NEC220 yields

233   only fractions containing equimolar amounts of UL31 and UL34, indicating the intact

234   UL31:UL34=1:1 complex [17]. Indeed, this pattern was observed for the NEC220-R139A$_{UL34}$

235   mutant **(Fig. S2a).** However, both NEC220-K137A$_{UL34}$ and NEC220-K137A$_{UL34}$/R139A$_{UL34}$

236   mutants also yielded fractions containing free UL34 or fractions containing more UL34 than

237   UL31 **(Fig. S2bc)** despite equimolar amounts of UL31 and UL34 being loaded onto the size-

238   exclusion column. Thus, the K137A$_{UL34}$ mutation appeared to destabilize the NEC heterodimer.

239   No free UL31 was detected in any of the fractions, suggesting that it may have been retained on

240   a filter within the chromatography line. Only fractions containing equimolar amounts of UL31

241   and UL34 were used for further characterization.

242
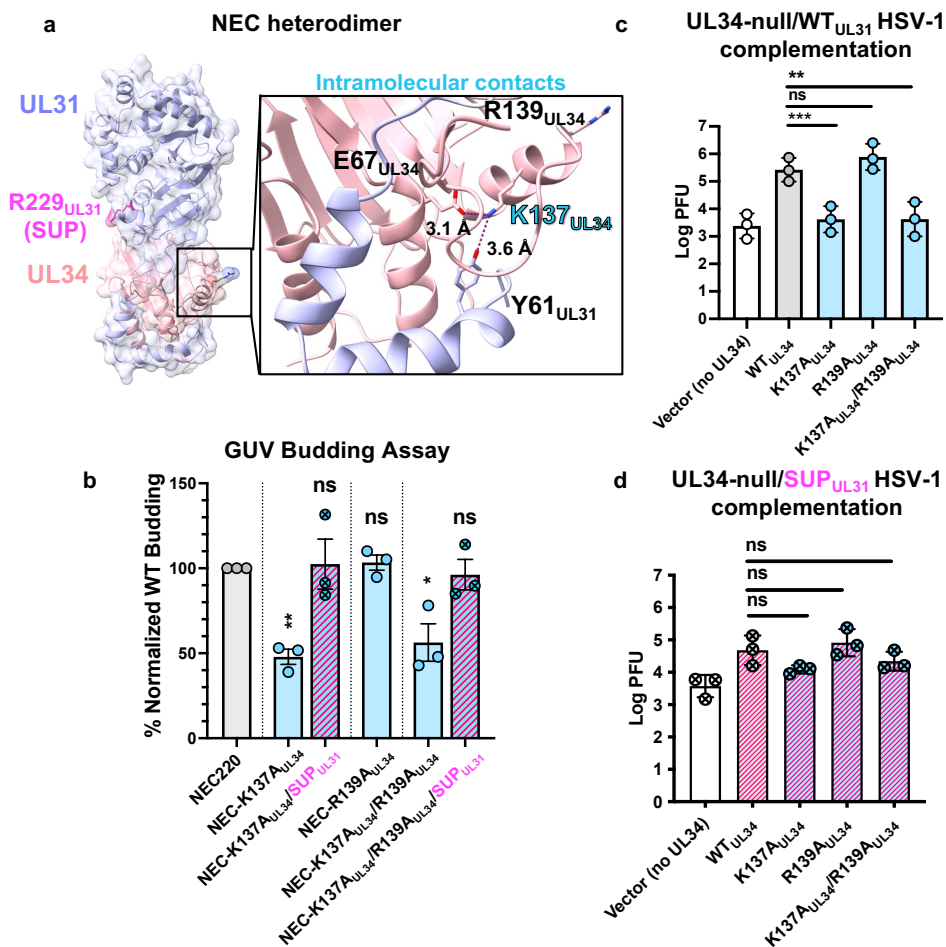
Fig. 3. The SUP$_{UL31}$ mutation restores budding to heterodimeric interface mutants and complements viral growth defects. a) Locations of intramolecular NEC residues mutated for this study. Inset shows interactions between various residues at the heterodimeric interface thought to be important for NEC heterodimer stabilization. **b)** NEC-SUP$_{UL31}$ rescues budding of NEC heterodimeric interface mutants *in vitro*. The percentage of *in-vitro* budding was determined by counting the number of ILVs within the GUVs after the
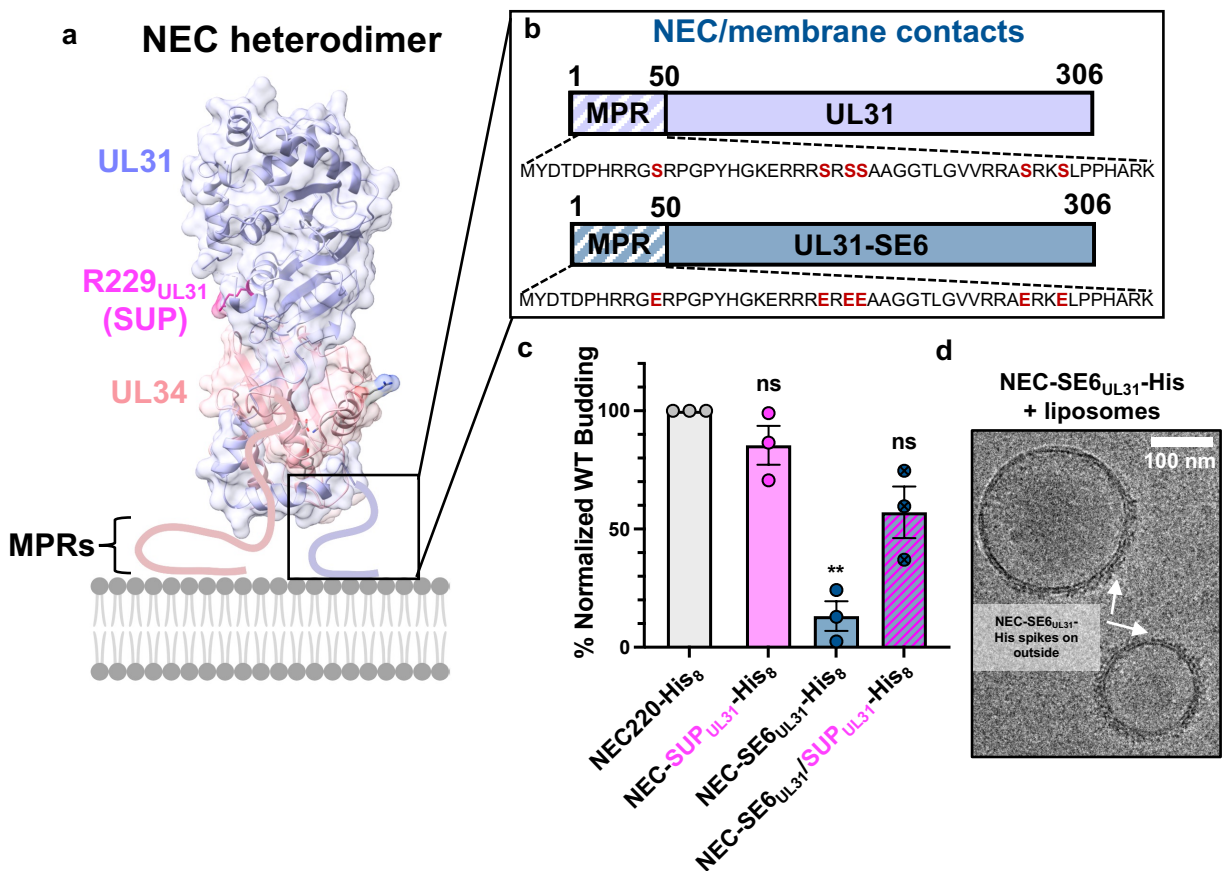
10

248   addition of NEC220 or the corresponding NEC mutant. A background count, the number of ILVs in the
249   absence of NEC, was subtracted from each condition. Each construct was tested in three biological replicates,
250   each consisting of three technical replicates. Symbols show the average budding efficiency of three technical
251   replicates compared to NEC220 (100%; grey). Significance was calculated using an unpaired Student's t-test
252   with Welch's correction ($P < 0.05$ = *; $P < 0.01$ = **; ns = not significant) in GraphPad Prism 9.0. **c)** WT$_{UL34}$
253   can only complement the growth of the R139A$_{UL34}$ heterodimeric interface mutant whereas SUP$_{UL31}$ **(d)** can
254   partially complement more. For both experiments, Hep-2 cells were transfected with the corresponding UL34
255   mutant plasmid and infected with a UL34-null/UL31 WT virus **(c)** or a UL34-null/UL31$_{R229L}$ virus **(d)**. Each
256   bar represents the mean of three independent experiments. Statistical significance was determined by
257   performing a one-way ANOVA on log-converted values using the Method of Tukey for multiple comparisons
258   implemented on GraphPad Prism. **, $P < 0.01$ = **; $P < 0.001$ = ***; ns, not significant.
259

260   Both K137A$_{UL34}$ and K137A$_{UL34}$/R139A$_{UL34}$ mutations reduced budding to ~50% of the

261   WT NEC220 whereas the R139A$_{UL34}$ mutation had no effect **(Fig. 3b)**. The K137A$_{UL34}$ mutation

262   is thus solely responsible for the defective budding phenotype of the double

263   K137A$_{UL34}$/R139A$_{UL34}$ mutant. Surprisingly, the SUP$_{UL31}$ mutation fully restored efficient

264   budding to both K137A$_{UL34}$ and K137A$_{UL34}$/R139A$_{UL34}$ mutants **(Fig. 3b).** But the mutant NEC

265   heterodimers remained unstable **(Fig. S3)**. Therefore, the SUP$_{UL31}$ mutation does not restore

266   budding by restoring heterodimer stability.

267   To assess the effects of these mutations on viral replication, we performed the viral

268   growth complementation assay described above. Both K137A$_{UL34}$ and R139A $_{UL34}$ proteins are

269   expressed at levels similar to WT **(Fig. S1)**. R139A$_{UL34}$ complemented the growth of both the

270   UL34-null **(Fig. 3c)** and UL34-null/SUP$_{UL31}$ viruses on par with the WT UL34 **(Fig. 3d).** As

271   expected, K137A$_{UL34}$ and K137A$_{UL34}$/R139A$_{UL34}$ complemented growth of the UL34-null virus

272   poorly **(Fig. 3c),** which is consistent with their *in-vitro* budding defects. However, both mutants

273   complemented the growth of the UL34-null/SUP$_{UL31}$ virus almost as efficiently as the WT UL34

274   **(Fig. 3d)**. Therefore, SUP$_{UL31}$ mutation can restore both budding and replication defects caused

275   by the K137A$_{UL34}$ mutation.

276

277   ***The SUP$_{UL31}$ mutation partially restores budding in vitro to a membrane interface mutant.*** In

278   addition to UL31/UL34 and NEC/NEC interfaces, the NEC/membrane interface is also

279   functionally important in HSV-1 NEC. Both UL31 and UL34 contain membrane-proximal

280   regions (MPRs) **(Fig. 4ab)** that mediate membrane association [17,27] and are essential for budding

281   *in vitro* [27]. The UL31 MPR contains clusters of positively charged residues that interact with

282   model membranes and increase lipid order, which leads to membrane deformation and budding

283   [27]. The UL31 MPR also contains six serines **(Fig. 4b)** that are phosphorylated during infection [5]

11

284   by the HSV-1 kinase US3 [29]. Phosphomimicking serine-to-glutamate mutations of these six

285   serines (SE6$_{UL31}$) **(Fig. 4b)** reduce nuclear egress and viral titers during HSV-1 infection [30] and

286   impair NEC/membrane interactions and budding activity *in vitro* [27]. Previously, we proposed that

287   negative charges introduced by phosphorylation or phosphomimicking mutations reduce

288   electrostatic interactions between the MPR and the lipid headgroups that are necessary for

289   membrane deformation and budding [27]. Here, we asked whether the SUP$_{UL31}$ mutation could

290   restore budding *in vitro* to the budding-deficient SE6$_{UL31}$ mutant.

291

292   **Fig. 4. The SUP$_{UL31}$ mutation partially restores budding to a membrane interface mutant. a-b)** Location
293   of membrane interface residues mutated for this study. **c)** NEC-SUP$_{UL31}$ partially rescues budding in the
294   membrane interface mutant *in vitro*. The percentage of *in-vitro* budding was determined by counting the
295   number of ILVs within the GUVs after the addition of NEC220-His or the corresponding NEC mutant. A
296   background count, the number of ILVs in the absence of NEC, was subtracted from each condition. Each
297   construct was tested in three biological replicates, each consisting of three technical replicates. Symbols show
298   the average budding efficiency of three technical replicates compared to NEC220-His$_8$ (100%; grey). The
299   NEC-SE6$_{UL31}$-His$_8$ data were previously reported in [27]. Significance was calculated using an unpaired
300   Student's t-test with Welch's correction (P < 0.01 = **; ns = not significant) in GraphPad Prism 9.0. **d)** Cryo-
301   EM of NEC-SE6$_{UL31}$-His$_8$ and large unilamellar vesicles (LUVs) shows that the SE6$_{UL31}$ mutations perturb
302   NEC oligomerization when bound to membranes.

303

304	The NEC220 construct typically used in the *in-vitro* budding assays is soluble and

305	depends on functional MPRs for membrane recruitment. Since the $SE6_{UL31}$ mutation reduces

306	NEC/membrane interactions, to bypass the defect in membrane recruitment, we used the

307	NEC220 variant construct that contains a His_8-tag at the C terminus of UL34 [17,27]. When used in

308	conjunction with membranes containing Ni-chelating lipids, the His_8-tag ensures that the

309	NEC220-His_8 is recruited to the membranes even when the MPR mutations preclude membrane

310	association. The *in-vitro* budding efficiency of NEC220-His_8 was similar to that of untagged

311	NEC220, suggesting that the C-terminal His_8-tag has no deleterious effect on the membrane

312	budding activity [17,27]. Previously, we showed that such artificial tethering does not override the

313	requirement for the MPR/membrane interactions and does not restore budding to MPR mutants

314	with budding defects [27].

315	By itself, the SUP_{UL31} mutation did not change the budding efficiency of NEC220-His_8

316	**(Fig. 4c)**, similar to the untagged NEC220 **(Fig. 1e).** As previously reported by our group,

317	$SE6_{UL31}$ mutation reduced *in-vitro* budding to ~10% of the WT NEC220-His_8 despite the ability

318	to interact with membranes due to the His_8-tag [27] **(Fig. 4c)**. Therefore, we performed a cryo-EM

319	analysis to examine NEC220-$SE6_{UL31}$-His_8 membrane interactions. NEC220-$SE6_{UL31}$-His_8 was

320	incubated with large unilamellar vesicles (LUVs) of similar composition to the GUVs used for

321	the budding assay and imaged with cryo-EM **(Fig. 4d)**. NEC220-$SE6_{UL31}$-His_8 formed

322	membrane-bound spikes on the outside of the LUVs **(Fig. 4d)**, but the internal protein coats

323	indicative of budding [17,19,28] were rarely observed. This is reminiscent of the behavior of the

324	oligomerization-deficient NEC-DN_{UL34} mutant previously reported by our group [17]. We conclude

325	that the $SE6_{UL31}$ mutations perturb NEC oligomerization, likely as the consequence of weakened

326	MPR/membrane interactions [27]. Surprisingly, the SUP_{UL31} mutation restored budding of the

327	$SE6_{UL31}$ mutant to ~50% of the WT NEC220-His_8 **(Fig. 4c).** Therefore, the SUP_{UL31} mutation

328	can rescue budding *in vitro,* even if partially, to a mutant that indirectly disrupts oligomerization

329	by weakening MPR/membrane interactions.

330	

331	**The *SUP_{UL31} mutation does not cause major conformational changes in the NEC heterodimer.***

332	To identify the mechanism by which the SUP_{UL31} mutation can restore budding to a broad range

333	of mutants, we first asked whether the SUP_{UL31} mutation influenced the NEC structure. We

334	crystallized the equivalent of the previously crystallized WT NEC185Δ50 construct (UL31: 51-

335   306 and UL34: 15-185) [22], which lacks the MPRs that impede crystallization and contains the

336   SUP_{UL31} mutation, NEC185Δ50-SUP_{UL31}. The NEC185Δ50-SUP_{UL31} structure was determined

337   using molecular replacement with the WT NEC185Δ50 structure as a search model and refined

338   to 3.9-Å resolution **(Supplementary Table S1).** NEC185Δ50-SUP_{UL31} took the space group $C2_1$

339   with six NEC heterodimers in the asymmetric unit **(Supplementary Table S1).** The atomic

340   coordinates and structure factors of the NEC185Δ50-SUP_{UL31} structure have been deposited to

341   the RCSB Protein Data Bank under the accession number 8G6D.

342   The six non-crystallographic NEC185Δ50-SUP_{UL31} heterodimers, SUP_{AB}, SUP_{CD}, SUP_{EF},

343   SUP_{GH}, SUP_{IJ}, and SUP_{KL} (UL34 chains: A, C, E, G, I, and K; UL31 chains: B, D, F, H, J, and

344   L) were well resolved (95-99% of all residues; **Supplementary Table S2**) and structurally

345   similar, with root mean square deviations (RMSDs) ranging from 0.67 to 1.00 Å

346   **(Supplementary Table S3).** By contrast, the equivalent WT NEC185Δ50 construct took the P6

347   space group with two crystallographically independent heterodimers in the asymmetric unit,

348   NEC_{AB} and NEC_{CD} (UL34 chains: A and C; UL31 chains: B and D) [22]. The overall structures of

349   the two WT NEC heterodimers and the six NEC-SUP_{UL31} mutant heterodimers are very similar.

350   They can be superimposed with RMSDs ranging from 0.83 to 1.02 Å **(Supplementary Table**

351   **S4)** and share similar heterodimeric interfaces **(Supplementary Table S5).** In four of the six

352   SUP mutant heterodimers (SUP_{AB}, SUP_{CD}, SUP_{EF}, and SUP_{KL}), residues 129-133 and 261-268 of

353   UL31, unresolved in the WT structure, were resolved **(Fig. S4).** All six copies of UL34 in the

354   NEC-SUP_{UL31} mutant contained additional density at the C terminus **(Fig. S4).** Importantly, the

355   location of residue at position 229, $R229_{UL31}$ in WT and $L229_{31}$ in SUP_{31}, is unchanged **(Fig. S4).**

356   Thus, the SUP_{UL31} mutation does not alter the NEC heterodimer structure in any major way.

357   To rule out the possibility that the SUP_{UL31} mutation altered the NEC structure only in the

358   presence of mutations causing budding defects, we also crystallized the NEC185Δ50-

359   DN_{UL34}/SUP_{UL31} construct. The NEC185Δ50-DN_{UL34}/SUP_{UL31} also took the $C2_1$ space group

360   with six heterodimers in the asymmetric unit but diffracted x-rays only to ~6 Å resolution. Given

361   the resolution, we did not perform an in-depth analysis on the NEC185Δ50-DN_{UL34}/SUP_{UL31}

362   mutant heterodimers within the crystals. Nonetheless, the similarities between the two constructs

363   (the formation of hexagonal crystals, the space group, and the number of heterodimers in the

364   asymmetric unit) suggest the DN_{UL34} mutations do not have a substantial effect on NEC crystal

365   packing and most likely do not alter NEC conformation.

366

WT NEC, NEC-SUP$_{UL31}$, and NEC-DN$_{UL34}$/SUP$_{UL31}$ form similar hexagonal arrays in vitro.

The WT NEC homologs from HSV-1, PRV, and HCMV oligomerize into hexagonal arrays [17,20-23]. HSV-1 NEC220 forms membrane-bound hexagonal coats on the inner surface of budded vesicles *in vitro* [17,28] whereas NEC185Δ50 forms flat hexagonal lattices of very similar dimensions in the crystals [22]. In the crystals of WT HSV-1 NEC185Δ50, the two independent NEC heterodimers, NEC$_{AB}$ and NEC$_{CD}$, form two very similar hexamers, hex$_{AB}$ and hex$_{CD}$, that are perfectly symmetrical due to the P6 crystal symmetry **(Fig. 5ab)** and have similar hexameric interfaces **(Supplementary Table S6)**. However, these two hexamers form two distinct hexagonal lattices **(Fig. 5ab)** [22]. In both lattices, interactions between the hexamers result in trimers formed by UL31/UL31 interactions **(Fig. 5ab, red)**. The hex$_{AB}$ lattice also has two types of dimers formed by either UL31/UL31 or UL31/UL34 interactions **(Fig. 5a, coral and gold, respectively)**. But the hex$_{CD}$ lattice has only one dimer type formed by UL31/UL34 interactions **(Fig. 5b, gold)**. The WT HSV-1 NEC hexamers can, thus, interact in more than one way.
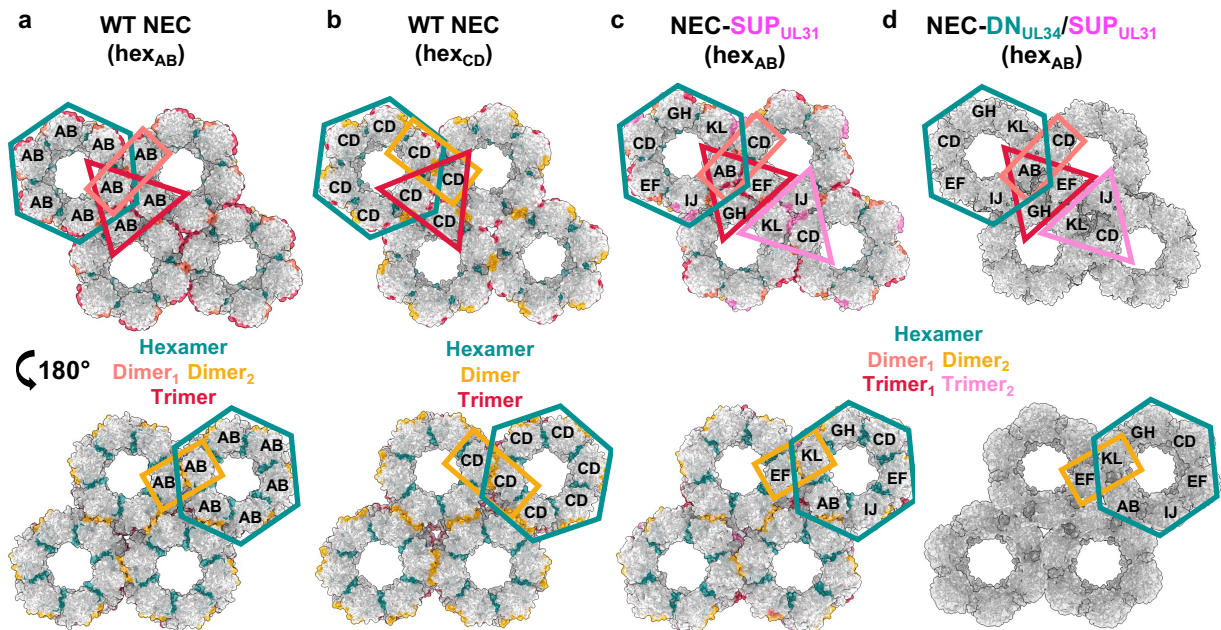
Fig. 5. NEC-SUP$_{UL31}$ and NEC-DN$_{UL34}$/SUP$_{UL31}$ form hex$_{AB}$ lattices in the crystals. a) The HSV-1 WT NEC hex$_{AB}$ (PDB ID: 4ZXS), **b)** the WT NEC hex$_{CD}$ (PDB ID: 4ZXS), **c)** the NEC-SUP$_{UL31}$ and **d)** the NEC-DN$_{UL34}$/SUP$_{UL31}$ crystal lattices [22]. Hexameric (teal) and interhexameric (dimer$_1$: coral, dimer$_2$: gold, trimer$_1$: red, and trimer$_2$: light pink) interfaces are colored accordingly. Two distinct trimers formed in the NEC-SUP$_{UL31}$ lattice (red and light pink). Due to resolution, an interface analysis was not performed on the NEC-DN$_{UL34}$/SUP$_{UL31}$ crystal lattice. The corresponding heterodimers within the lattice are labeled.

387

388   To understand how the SUP_{UL31} mutation may suppress budding defects, we examined

389   the oligomeric arrays formed by NEC-SUP_{UL31} in the crystals and membrane-bound coats. The

390   NEC185Δ50-SUP_{UL31} also forms hexamers in the crystals, but in this case, the hexamers are

391   asymmetrical, being formed by six independent, non-crystallographic heterodimers in the

392   asymmetric unit **(Fig. 5C).** Nonetheless, the NEC185Δ50-SUP_{UL31} hexamers look very similar to

393   the WT NEC185Δ50 hexamers, with similar hexameric interfaces **(Supplementary Table S6)**,

394   85-97% in identity **(Supplementary Table S7)**. The SUP_{UL31} mutation thus has no major effect

395   on the hexamer structure. The crystal lattice formed by the NEC185Δ50-SUP_{UL31} hexamers **(Fig.**

396   **5c)** resembles the WT NEC hex_{AB} lattice **(Fig. 5a; Supplementary Tables S8-S10).** The

397   NEC185Δ50-DN_{34}/SUP_{31} crystal lattice also resembles the WT NEC hex_{AB} lattice **(Fig. 5d).**

398   To examine the effect of the SUP_{UL31} mutation on the geometry of the membrane-bound

399   NEC coats, we performed cryo-EM/T analyses on WT NEC220 and the mutants NEC220-

400   SUP_{UL31} and NEC220-DN_{UL34}/SUP_{UL31}. Each protein complex was incubated with LUVs,

401   similar in composition previously used to visualize the WT NEC220 coats on budded vesicles

402   [17,19,28]. The budded vesicles formed by NEC220-SUP_{UL31} were prone to aggregation, which

403   reduced the number of NEC220-SUP_{UL31} particles available for data processing, resulting in a

404   lower final resolution compared to WT NEC220 and NEC220-DN_{UL34}/SUP_{UL31}. Sub-

405   tomographic averaging of the 3D reconstructions of either WT NEC220 (5.9 Å), NEC220-

406   SUP_{UL31} (13.1 Å), or NEC220-DN_{UL34}/SUP_{UL31} (5.4 Å) revealed that all three constructs formed

407   very similar hexameric lattices **(Fig. 6a-c; Supplementary Table S11)** resembling the WT NEC

408   hex_{CD} crystal lattice **(Fig. 5b).**

409   The higher resolution of the WT NEC220 and NEC220-DN_{UL34}/SUP_{UL31} averaged cryo-

410   ET density map allowed us to dock the crystal structure of the WT NEC185Δ50 heterodimer

411   **(Figs. 6df),** confirming that the SUP_{UL31} mutation does not perturb NEC conformation, even

412   when bound to membranes. We also observed additional helical density at the C terminus of

413   UL34, corresponding to helix α4 that was unresolved in the WT NEC185Δ50 crystal structure [22]

414   but present in the crystal structures of NEC homologs from PRV[22,31], HCMV[23,32], and EBV [19].

415   The PRV UL34 α4 helix fit well into the HSV-1 UL34 cryo-ET averages **(Figs. 6eg)**.

416   Interestingly, in the crystals, the WT NEC220 formed both hex_{AB} and hex_{CD} lattices

417   whereas the mutants formed only the hex_{AB} lattice. However, in the membrane-bound coats, the

418   WT NEC220 and both mutants formed only the hex_{CD} lattice. The reasons for these differences

419 are yet unclear. Regardless, just as the WT NEC, both NEC-SUP$_{UL31}$ and NEC-DN$_{UL34}$/SUP$_{UL31}$

420 mutants can form either type of lattice. Therefore, the SUP$_{UL31}$ mutation does not promote the

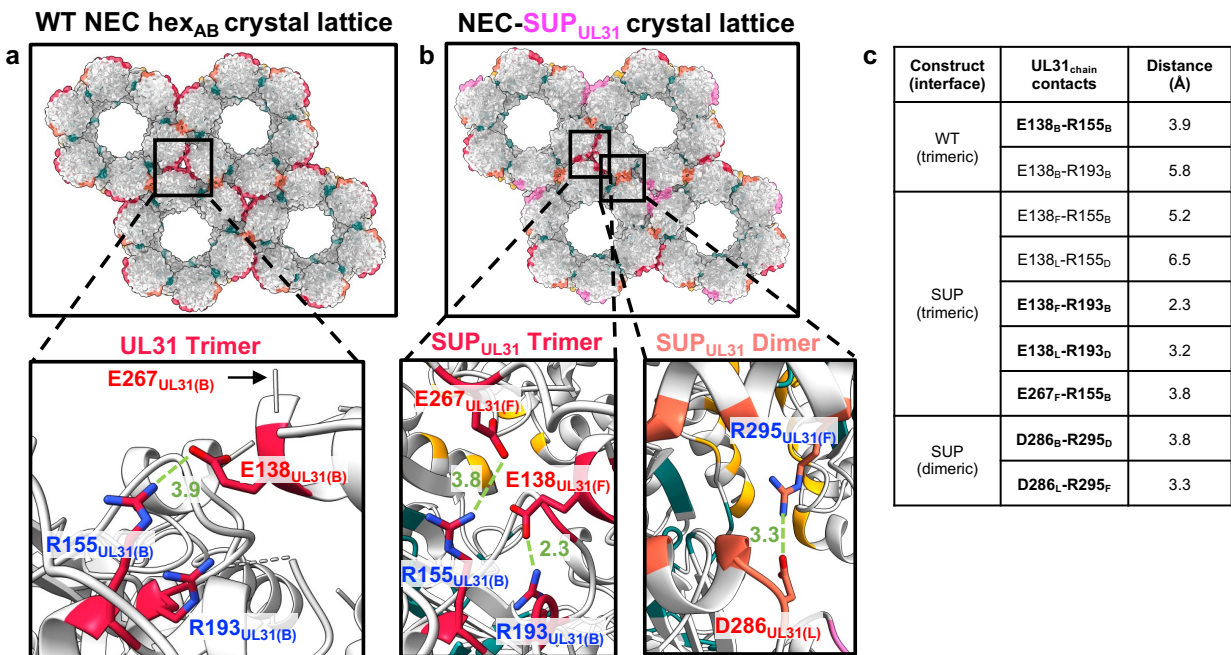421 formation of a different NEC lattice type.

422

423
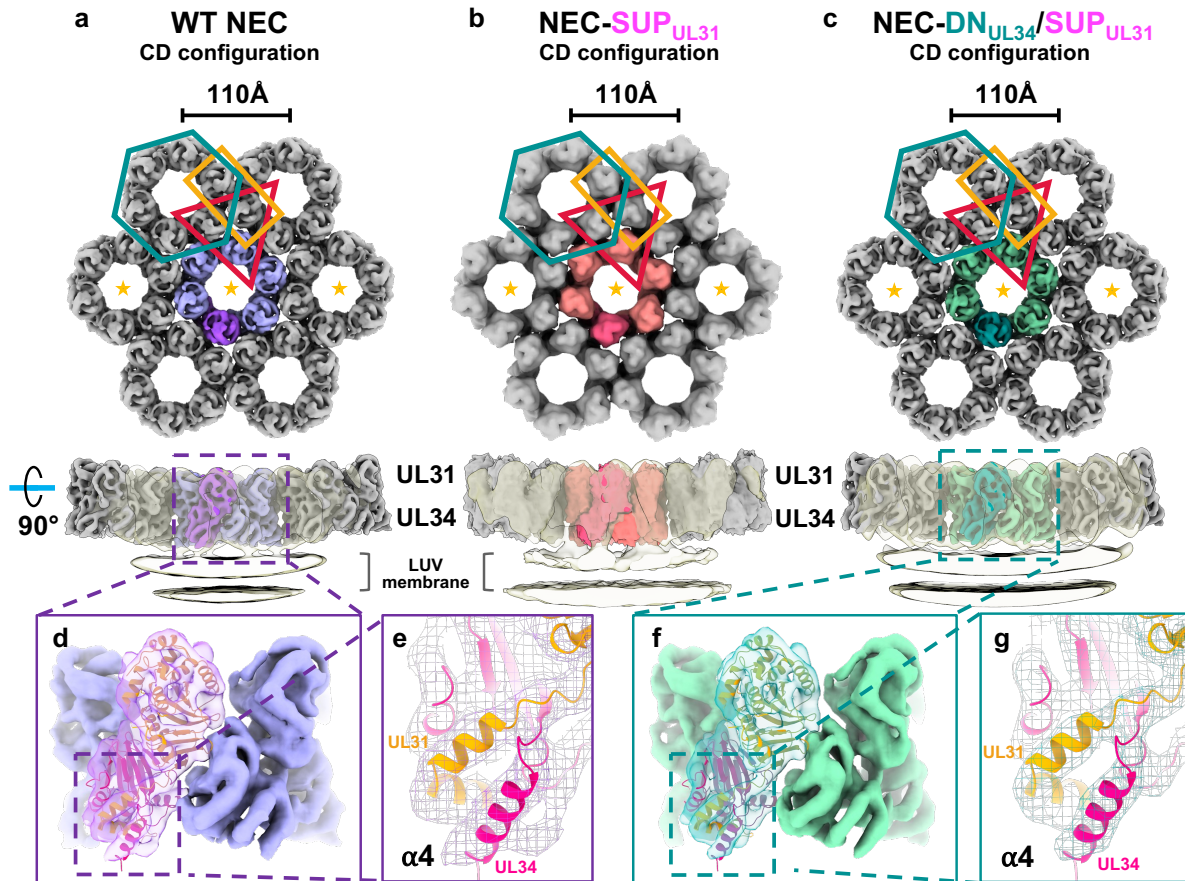
Fig. 6. WT NEC, NEC-SUP$_{UL31}$, and NEC-DN$_{UL34}$/SUP$_{UL31}$ form hex$_{CD}$ membrane-bound coats. Cryo-ET reconstruction of **a)** the WT NEC coat at 5.9 Å, **b)** the NEC-SUP$_{UL31}$ coat at 13.1 Å, and **c)** the NEC-DN$_{UL34}$/SUP$_{UL31}$ coat at 5.4 Å. Only the three hexameric units marked with orange stars are shown in lower 90°-rotated panels, where the low-pass filtered transparent densities show the connection between NEC lattices and LUV membrane. The HSV-1 NEC crystal structure (PDB ID: 4ZXS) docks similarly into both the WT NEC **(d)** and NEC-DN$_{UL34}$/SUP$_{UL31}$ **(f)** cryo-ET densities. **e, g)** Docking of the α4 helix from the PRV NEC crystal structure (PDB ID: 4Z3U) accounts for the additional density observed in both cryo-ET reconstructions which was originally unresolved in the HSV-1 NEC crystal structure[22].

432

The SUP$_{UL31}$ mutation generates new contacts at the interhexameric interface. To determine

434 whether the SUP$_{UL31}$ mutation changed any contacts at the lattice interfaces, we analyzed the

435 buried surface areas and sidechain contacts (hydrogen bonds and salt bridges) in the WT NEC

436 and NEC-SUP$_{UL31}$ crystal structures using PiSA interface analysis [33]. We found that the buried

437 surface area at 5/6 hexameric interfaces in the NEC-SUP$_{UL31}$ crystal lattice was ~15% smaller
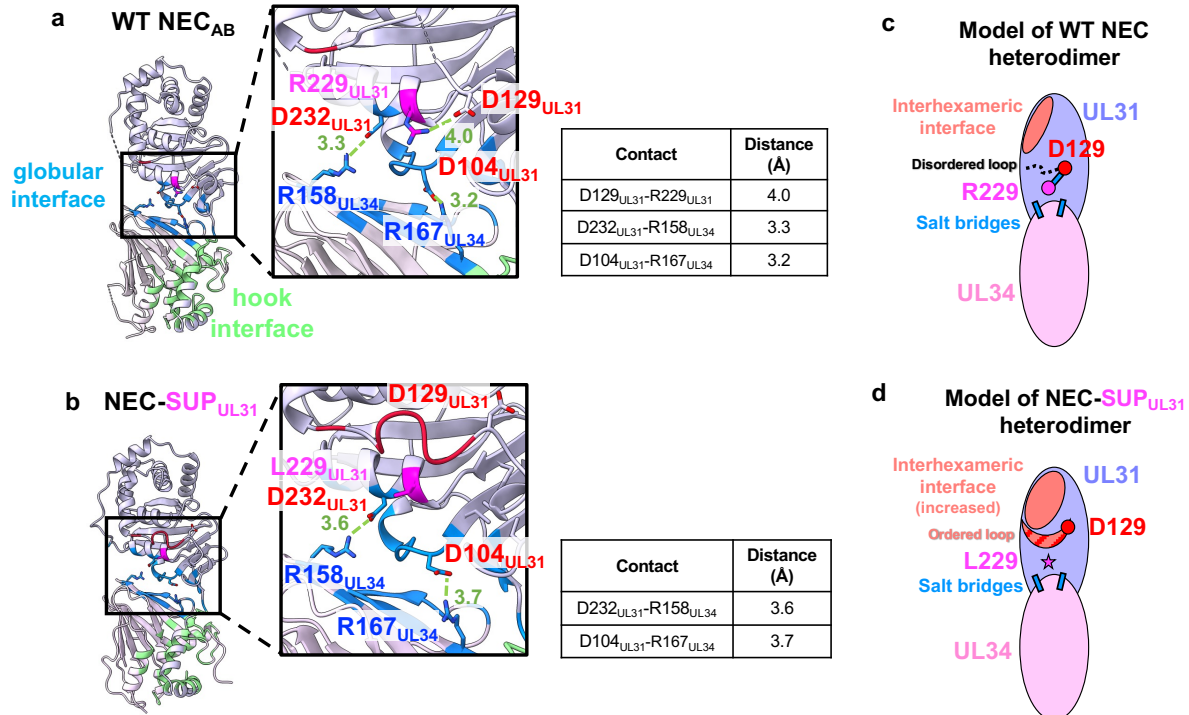
17

438   compared to the WT NEC hex_{AB} and hex_{CD} lattices **(Supplementary Table S12)** and that the

439   number of hydrogen bonds and salt bridges was also reduced **(Supplementary Table S13).** The

440   remaining hexameric interface, A/K, had more contacts than the WT **(Supplementary Table**

441   **S13).** Thus, the SUP_{UL31} mutation appears to alter contacts at the hexameric interfaces.

442   By contrast, the buried surface area at the interhexameric interfaces was larger in the

443   NEC-SUP_{UL31} crystal lattice **(Supplementary Table S14)** and had additional interactions absent

444   from the WT NEC lattice **(Supplementary Table S15).** For example, the trimeric interface in

445   the WT NEC hex_{AB} lattice has one salt bridge, $E138_{UL31}$-$R155_{UL31}$ **(Fig. 7a).** The NEC-SUP_{UL31}

446   lattice has two trimeric interfaces, B/F/H and D/J/L. In both, $E138_{UL31}$ forms a salt bridge with

447   another residue, $R193_{UL31}$ **(Fig. 7b).** $R155_{UL31}$ forms a salt bridge with $E267_{UL31}$, but only in the

448   B/F/H trimer **(Fig. 7b).** In the D/J/L trimer, these residues are ~7 Å apart. $E267_{UL31}$ was

449   unresolved in the WT NEC_{AB} structure, but its side chain is too far away from the interhexameric

450   interface to participate in any contacts **(Fig. 7a)**. As another example, there is a new salt bridge,

451    $D286_{UL31}$-$R295_{UL31}$, at the NEC-SUP_{UL31} dimeric interfaces B/D and F/L **(Fig. 7b),** which is

452   absent from the WT NEC lattice. Therefore, the NEC-SUP_{UL31} mutation causes the formation of

453   additional contacts at the interhexameric interface that could ostensibly stabilize the NEC lattice

454   even in the presence of lattice-destabilizing mutations. New interhexameric contacts likely also

455   form in the hex_{CD} lattice, but in the absence of higher resolution data, what residues participate in

456   these contacts is unknown.

457

WT NEC hex_{AB} crystal lattice   **NEC-SUP_{UL31} crystal lattice**

a   b

UL31 Trimer   **SUP_{UL31} Trimer**   **SUP_{UL31} Dimer**

Construct (interface)	UL31$_{chain}$ contacts	Distance (Å)
WT (trimeric)	**$E138_B$-$R155_B$**	3.9
	$E138_B$-$R193_B$	5.8
SUP (trimeric)	$E138_F$-$R155_B$	5.2
	$E138_L$-$R155_D$	6.5
	$E138_F$-$R193_B$	2.3
	$E138_L$-$R193_D$	3.2
	$E267_F$-$R155_B$	3.8
SUP (dimeric)	**$D286_B$-$R295_D$**	3.8
	$D286_L$-$R295_F$	3.3

18

Fig. 7. The interhexameric interfaces in WT NEC hex$_{AB}$ and NEC-SUP$_{UL31}$ lattices have different contacts. Close-up views of the interhexameric interfaces in the **(a)** WT NEC crystal lattice (UL31 trimer; crimson) and **(b)** NEC-SUP$_{UL31}$ crystal lattice [UL31 trimers (crimson and pink) and dimers (orange and yellow)]. The HSV-1 NEC crystal structure (PDB: 4ZXS) was used to generate the figure in panel **a**. Salt bridges are shown as green dashed lines, with distances in Angstrom. Residues forming salt bridges are shown as sticks and colored in blue (Rs) or red (Es and Ds). **c)** Distances of contacts at the highlighted interfaces. Contacts in bold are salt bridges.

a **WT NEC$_{AB}$**

Contact	Distance (Å)
D129$_{UL31}$-R229$_{UL31}$	4.0
D232$_{UL31}$-R158$_{UL34}$	3.3
D104$_{UL31}$-R167$_{UL34}$	3.2

c **Model of WT NEC heterodimer**

b **NEC-SUP$_{UL31}$**

Contact	Distance (Å)
D232$_{UL31}$-R158$_{UL34}$	3.6
D104$_{UL31}$-R167$_{UL34}$	3.7

d **Model of NEC-SUP$_{UL31}$ heterodimer**

Fig. 8. The SUP$_{UL31}$ mutation introduces changes to the heterodimeric interface. The crystal structures of **(a)** WT NEC$_{AB}$ and **(b)** NEC-SUP$_{UL31}$ heterodimers. The heterodimeric interface residues are colored blue (globular interface) or green (hook interface). Residue 229$_{UL31}$ is colored magenta. Insets show close-up views of the globular interface. Residues forming salt bridges at the interface are shown as sticks and colored in blue (Rs) or red (Es and Ds). Residue 229$_{UL31}$ is shown as sticks and colored in magenta. Salt bridges are shown as dashed green lines, with distances in Angstrom. Distances are also listed in the corresponding tables. The resolved portions of the dynamic loop 129$_{UL31}$-134$_{UL31}$ are shown in red. The HSV-1 NEC crystal structure (PDB: 4ZXS) was used to generate the figure in **(a)**. Corresponding cartoon models of either the **(c)** WT NEC or **(d)** NEC-SUP$_{UL31}$ heterodimeric interfaces.

The SUP$_{UL31}$ mutation generates new interface contacts indirectly by eliminating a salt bridge.

While residue 229$_{UL31}$ does not participate in any interface contacts directly, it is located right above the heterodimeric globular interface **(Fig. 8a)**. In the WT NEC$_{AB}$ structure, the R229$_{UL31}$ side chain makes a salt bridge with the nearby D129$_{UL31}$. D129$_{UL31}$ is located at one end of a mostly disordered loop, residues 129$_{UL31}$-134$_{UL31}$ **(Fig. 8ac)**, that was only partially resolved in the WT NEC$_{AB}$ structure and unresolved in the WT NEC$_{CD}$ structure. The R229L$_{UL31}$ mutation

483   eliminates the salt bridge, and in all SUP_{UL31} heterodimers (except for SUP_{KL} where it was

484   unresolved), the $D129_{UL31}$ side chain points away from $L229_{UL31}$ **(Fig. 8b).** Interestingly, in the

485   NEC-SUP_{UL31} structure, the 129_{UL31}-134_{UL31} loop is better ordered. It was fully resolved in four

486   out of six NEC-SUP_{UL31} heterodimers **(Fig. 8d, red)** and partially resolved in the remaining two

487   **(Supplementary Table S9).** Moreover, this loop also participates in new contacts at the

488   interhexameric interface in five out of the six NEC-SUP_{UL31} heterodimers, **(Supplementary**

489   **Table S9).** To sum up, in the NEC-SUP_{UL31}, the lack of the $R229_{UL31}$-$D129_{UL31}$ salt bridge

490   correlates with a more ordered 129_{UL31}-134_{UL31} loop **(Fig. 8bd, red)** and a larger interhexameric

491   interface **(Fig. 8d)**. Therefore, we hypothesize that by eliminating the salt bridge, the SUP_{UL31}

492   mutation releases the loop, which then forms new contacts at the interhexameric interface.

493

494   **DISCUSSION**

495   Herpesviruses translocate their capsids from the nucleus to the cytoplasm by an unusual

496   mechanism that requires the formation of membrane-bound coats by the virally encoded

497   heterodimeric complex, the NEC [17,20,21]. The coats are composed of a hexagonal NEC lattice, and

498   mutations that disrupt the lattice interfaces reduce budding *in vitro* [17,22,27] and viral replication [24-

499   26,30], attesting to its central role in the NEC membrane-budding function. Here, we demonstrated

500   that a suppressor mutation within the UL31 protein, SUP_{UL31}, restored efficient membrane

501   budding *in vitro* and viral replication to a broad range of budding-deficient NEC mutants. The

502   SUP_{UL31} mutation thus acts as a universal suppressor of membrane budding defects in NEC.

503   Furthermore, we found that the SUP_{UL31} mutation expanded lattice interfaces by indirectly

504   creating new interface contacts. We hypothesize that the SUP_{UL31} mutation exerts its powerful

505   suppressor effect by stabilizing the hexagonal coats destabilized by mutations.

506

507   ***The SUP_{UL31} mutation promotes the formation of new interhexameric contacts.*** Since the

508   SUP_{UL31} mutation rescued budding defects caused by disruptions of the hexagonal lattice, we

509   initially hypothesized that it may do so promoting the formation of a different, potentially, non-

510   hexagonal lattice with distinct interfaces. Instead, we found that NEC-SUP_{UL31} and NEC-

511   DN_{UL34}/SUP_{UL31} mutants formed hexagonal lattices both in the crystals and in membrane-bound

512   coats that were very similar to those formed by the WT NEC. However, the interhexameric

513   interfaces in the NEC-SUP_{UL31} crystal lattice are larger due to several new interactions,

514   particularly, salt bridges. The SUP_{UL31} mutation does not participate in any interface contacts

515   itself. Instead, we hypothesize that it promotes new interface contacts indirectly by eliminating

516   the $R229_{UL31}$-$D129_{UL31}$ salt bridge **(Fig. 8b)**. This releases the 129_{UL31}-134_{UL31} loop, which

517   becomes better ordered **(Fig. 8d)** and forms new contacts at the interhexameric interface **(Fig.**

518   **7b).** Larger interhexameric lattice interfaces would be expected to reinforce the lattice. By

519   stabilizing the lattice disrupted by mutations, the SUP_{UL31} mutation could restore efficient

520   budding.

521   It is easy to envision how the SUP_{UL31} mutation might suppress budding defects caused

522   by mutations that destabilize interhexameric interactions by compensating for the loss of those

523   interactions locally with new interhexameric interactions. However, the SUP_{UL31} mutation also

524   suppresses budding defects of mutants that destabilize the hexamers themselves. Therefore, we

525   propose a more general mechanism for this type of suppression. We suggest that the NEC

526   hexamers weakened by interface mutations can be stabilized not only by the interactions between

527   adjacent NEC heterodimers within the hexamer itself but also by their incorporation into a larger

528   lattice where interhexameric contacts would limit the dissociation of NEC heterodimers from the

529   hexamer **(Fig. 9)**. By strengthening these latter contacts, the SUP_{UL31} mutation can thereby

530   compensate for different kinds of lattice defects.

NEC lattice formation (top view)
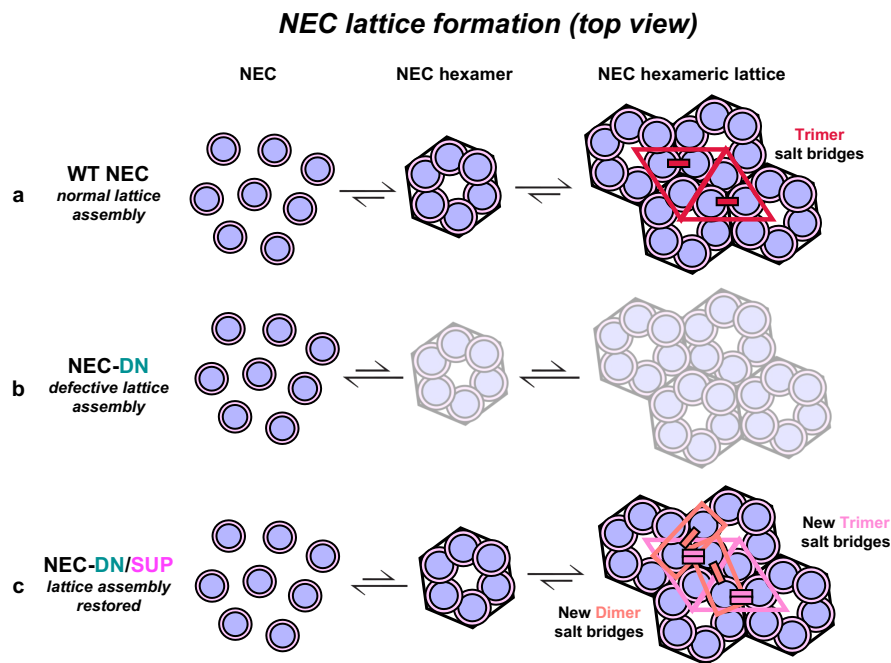
SUP overrides the deleterious effects of lattice-disrupting mutations by indirectly promoting new contacts that stabilize the hexagonal lattice

531

Fig. 9. A model of SUP$_{UL31}$ budding restoration in the context of a lattice destabilizing mutation. a) WT NEC heterodimers arrange into hexamers that build into a stable hexameric lattice by forming contacts at the hexameric and interhexameric interfaces. The salt bridges located at the interhexameric interface trimers (crimson) favor lattice association, rather than disassociation. In the presence of a lattice destabilizing mutation such as NEC-DN$_{UL34}$ **(b)**, hexamer formation and lattice assembly are perturbed. In contrast, the SUP$_{UL31}$ mutation **(c)** restores lattice formation by promoting the formation of new contacts at both the dimeric and trimeric interhexameric interfaces (pink and salmon), resulting in a stable and functional NEC lattice, despite the presence of a destabilizing mutation.

The SUP$_{UL31}$ mutation makes the NEC more conformationally dynamic. The WT NEC185Δ50 crystallized in the P6 space group, in which the hexamers are perfect, being related by crystallographic symmetry. However, both the NEC185Δ50-SUP$_{UL31}$ and NEC185Δ50-DN$_{UL34}$/SUP$_{UL31}$ mutants crystallized in the C2$_1$ space group, in which the hexamers are non-crystallographic and, thus, imperfect. This suggested that the NEC heterodimer becomes more conformationally dynamic in the presence of the SUP$_{UL31}$ mutation. Indeed, the heterodimeric UL31/UL34 interface between the globular cores of UL31 and UL34 buries a ~6-20% larger surface area in all six NEC-SUP$_{UL31}$ heterodimers compared to the WT NEC heterodimers **(Fig. S4, blue; Supplementary Table S16),** suggesting flexibility at this interface.

Residue 229$_{UL31}$ is located between two intermolecular salt bridges at the heterodimeric interface formed by the UL31 and UL34 globular cores, R158$_{UL34}$-D232$_{UL31}$ and R167$_{UL34}$-D104$_{UL31}$ **(Fig. 8b).** Previous molecular dynamics (MD) study proposed that these salt bridges contribute to the overall stability of the HSV-1 NEC heterodimer [34]. The HCMV NEC, which has only one salt bridge, was found to be more dynamic than HSV-1 in MD simulations[34]. The EBV NEC, which also has only one salt bridge, is a conformationally dynamic heterodimer as revealed by its crystal structure [19]. The number of intermolecular salt bridges at the globular UL31/UL34 interface thus correlates with the stability of the NEC heterodimer.

We propose that the intramolecular salt bridge R229$_{UL31}$-D129$_{UL31}$ is another important contributor to the stability of the NEC heterodimer. Although the NEC-SUP$_{UL31}$ still has two intermolecular salt bridges at the heterodimeric interface, it lacks the intramolecular salt bridge **(Fig. 8b)**, which increases its flexibility. This increased flexibility could explain why both NEC-SUP$_{UL31}$ and NEC-DN$_{UL34}$/SUP$_{UL31}$ required extra additives and small molecules (from the Silver Bullets) to form crystals relative to the WT NEC [22] and why both NEC-SUP$_{UL31}$ and NEC-DN$_{UL34}$/SUP$_{UL31}$ took the lower symmetry space group C2$_1$, rather than P6.

Despite the proposed variations in flexibility among closely related NECs, only two types of lattice configurations have been observed, hex$_{AB}$ and hex$_{CD}$. HSV-1 NEC, be it the WT or the

567 two mutants presented in this study, formed either hex_{AB} (WT-NEC, NEC-SUP_{UL31}, and NEC-

568 DN_{UL34}/SUP_{UL31}) or hex_{CD} (WT-NEC) lattice configurations in crystals and only hex_{CD} lattice in

569 membrane-bound coats. HCMV NEC packed into a hexagonal lattice resembling the hex_{CD}

570 lattice configuration [23]. Conversely, PRV NEC formed a hexagonal lattice resembling the hex_{AB}

571 lattice configuration in membrane-bound coats [20]. HCMV and PRV NEC homologs could, in

572 principle, adopt alternative configurations, hex_{AB} or hex_{CD}, respectively, under different

573 experimental conditions. Regardless, how the NEC assembles into a hexameric lattice of either

574 configuration is still unknown. The two different lattice types could be assembled via different

575 routes, yet their biological relevance is still unclear.

576

577 ***The SUP_{UL31} mutation acts as a universal suppressor against mutations disrupting the NEC***

578 ***budding activity.*** The SUP_{UL31} mutation was initially identified as an extragenic suppressor of a

579 nuclear budding defect caused by a double mutation within UL34, $D35A_{UL34}$/$E37A_{UL34}$

580 (DN_{UL34}), in HSV-1 infected cells [25]. Subsequently, we showed that the DN_{UL34} mutation blocks

581 the formation of the hexagonal NEC lattice [17] by eliminating important polar contacts at the

582 hexameric interface [22] and that the SUP_{UL31} mutation restored effective membrane budding *in*

583 *vitro* to the DN_{UL34} and another hexameric interface mutant, $V92F_{UL34}$ [22]. Here, we found that the

584 SUP_{UL31} mutation could restore budding to many lattice interface mutants ($T123Q_{UL34}$,

585 $F252Y_{UL31}$, and $E153R_{UL31}$; **Fig. 1**); the heterodimeric interface mutants ($K137A_{UL34}$ and

586 $K137A$/$R139A_{UL34}$; **Fig. 3**); and even to a membrane interface mutant ($SE6_{UL31}$; **Fig. 4**). Thus,

587 the SUP_{UL31} mutation acts a universal suppressor mutation that restores efficient budding *in vitro*

588 and, in several cases, viral replication to a diverse range of budding-deficient NEC mutants.

589 Although mutations that cause budding defects target diverse interfaces, all are expected

590 to destabilize the hexagonal NEC lattice, which is essential for the membrane budding process.

591 The destabilizing effect of the lattice interface mutations is the most apparent. But mutations

592 destabilizing the NEC heterodimer would also be expected to weaken the lattice by destabilizing

593 its core building block. Finally, NEC/membrane interactions likely destabilize the lattice within

594 the membrane-bound NEC coat indirectly. By reinforcing the lattice, the SUP_{UL31} mutation could

595 overcome these lattice destabilizing defects regardless of their nature.

596 In some cases, the SUP_{UL31} mutation could fully restore the *in-vitro* budding activity but

597 not viral replication, e.g., in the presence of the $T123Q_{UL34}$ and $E153R_{UL31}$ **(Fig. 2)**. We

598   hypothesize that these mutations may perturb the NEC functions that do not involve membrane

599   deformation, e.g., nuclear lamina dissolution, capsid docking at the INM, or capsid recruitment.

600   Thus, the SUP_{UL31} mutation specifically restores budding defects.

601   If the SUP_{UL31} mutation forms a stronger hexagonal lattice, why isn't this mutation

602   positively selected? We hypothesize that this mutation may impair other functions of the NEC.

603   This idea is supported by the observation that in the *in-trans* complementation experiment, viral

604   replication in the presence of the SUP_{UL31} mutation does not reach the WT levels **(Fig. 2).** While

605   the SUP_{UL31} mutation is not positively selected, it provides the virus with a strategy to maintain

606   replication in the presence of external stressors such as inhibitors targeting the NEC. Further

607   work to identify and characterize other herpesviral suppression mechanisms could aid in the

608   advancement of novel herpesviral therapeutics.

609

610   **MATERIALS AND METHODS**

611   ***Cells and viruses.*** Vero and Hep-2 cells were maintained as previously described [9]. The

612   properties of HSV-1(F) and vRR1072(TK+) (a UL34-null virus derived by homologous

613   recombination with HSV-1(F) have also been previously described [9,35]. The UL34-null virus and

614   the UL34-null/SUP_{UL31} recombinant viruses used for complementation assays were derived from

615   the pYEbac102 clone of the HSV-1 strain (F) genome in the bacterial strain GS1783 (a gift from

616   G. Smith, Northwestern U.) [36-38] as previously described. All UL34-null viruses were propagated

617   on Vero tUL34 CX cells that express HSV-1 pUL34 under the control of its native promoter

618   regulatory sequences [39]. Vero tUL34 CX cells were propagated in DMEM high glucose

619   supplemented with 5% fetal bovine serum and the antibiotic penicillin and streptomycin.

620

621   ***Cloning.*** All primers used for cloning are listed in **Supplementary Table S17**. Cloning of UL31

622   (1-306), UL34 (1-220), UL34 (15-185), UL34-His$_8$ (1-220 with a C-terminal His$_8$-tag) and the

623   corresponding UL31 and UL34 mutants [R229L$_{UL31}$ (SUP_{UL31}), D35A$_{UL34}$/E37A$_{UL34}$ (DN$_{UL34}$),

624   E37A$_{UL34}$, T123Q$_{UL34}$, F252Y$_{UL31}$, and E153R$_{UL31}$, and S11E$_{UL31}$/S24E$_{UL31}$/S26E$_{UL31}$/S27E

625    $_{UL31}$/S40E$_{UL31}$/S43E$_{UL31}$ (SE6$_{UL31}$)] was previously described [17,22,27].

626   *Oligomeric interface mutants.* Site-directed mutagenesis of pJB14 (UL31 1-306

627   R229L$_{UL31}$) was performed using splicing-by-overlap extension protocol followed by restriction

628   digest into the pKH90 plasmid (containing an N-terminal His-SUMO-PreScission tag in-frame

24

629   with a BamHI restriction site) to create either the F252Y$_{UL31}$/R229L$_{UL31}$ (pED20) or

630   E153R$_{UL31}$/R229L$_{UL31}$ (pED21) double mutants.

631   *Heterodimeric interface mutants.* Site-directed mutagenesis of pJB02 (UL34 1-220) was

632   performed using splicing-by-overlap-extension protocol followed by restriction digest into the

633   pJB02 plasmid (containing an N-terminal GST-PreScission tag in-frame with a SalI restriction

634   site) to create either the K137A$_{UL34}$ (pED25), R139A$_{UL34}$ (pED26), or the K137A$_{UL34}$/R139A$_{UL34}$

635   (pED27) mutants.

636   *Membrane interface mutants.* Site-directed mutagenesis of pJB60 (UL31-SE6$_{UL31}$ 1-306)

637   was performed using an inverse PCR protocol followed by blunt-end ligation to create the

638   SE6$_{UL31}$/R229L$_{UL31}$ mutant (pED45).

639   *Crystallization constructs.* Digested PCR fragments containing R229L$_{UL31}$Δ50-306 were

640   amplified from pJB114 (UL31 1-306 R229L$_{UL31}$) and subcloned by restriction digest into a

641   pET24b(+) plasmid harboring an N-terminal His$_6$-SUMO-PreScission tag in-frame with a

642   BamHI restriction site plasmid to create the R229L$_{UL31}$Δ50-306 plasmid (pXG20). Digested PCR

643   fragments containing D35A$_{UL34}$/E37A$_{UL34}$ were amplified from pJB06 (UL34 1-246

644   D35A$_{UL34}$/E37A$_{UL34}$) and subcloned by restriction digest into a pGEX-6P1 vector containing an

645   N-terminal GST-PreScission tag in-frame with a SalI restriction site to create the UL34 15-185

646   D35A$_{UL34}$/E37A$_{UL34}$ plasmid (pJB66).

647   *Cell complementation constructs.* Plasmid pRR1072Rep, which was the parent vector for

648   UL34 mutant plasmids used for cell culture complementation assays has been previously

649   described [26]. Mutant derivatives of pRR1072Rep that carry the D35A$_{UL34}$/E37A$_{UL34}$ and

650   K137A$_{UL34}$/R139A$_{UL34}$ double mutations have also been previously described and were referred

651   to as CL04 and CL10 in that publication [26]. Derivatives of pRR1072Rep containing the single

652   D35A$_{UL34}$, E37A$_{UL34}$, T123Q$_{UL34}$, K137A$_{UL34}$, and R139A$_{UL34}$ were constructed by Gibson

653   assembly. Plasmids were assembled from two PCR products, each generated using pRR1072Rep

654   as a template and using either a mutagenic forward primer paired with a reverse primer from the

655   ampicillin resistance gene, or a mutagenic reverse primer paired with a forward primer from the

656   ampicillin resistance genes. PCR products were digested with DpnI to remove template

657   sequences and then assembled using the New England BioLabs 2X Gibson assembly master mix

658   according to the manufacturer's instructions.

659

660 ***Expression and purification of WT NEC, oligomeric interface, and heterodimeric interface***

661 ***mutants.*** Plasmids encoding HSV-1 UL31 1-306 (pKH90) and UL34 1-220 were co-transformed

662 into *Escherichia coli* BL21(DE3) LoBSTr cells (Kerafast) to generate wild-type NEC220 [17,28].

663 All mutant constructs contained UL31 1-306 and UL34 1-220 amino acid boundaries. Plasmids

664 encoding the appropriate mutations of either UL31 or UL34 were also co-transformed into *E.*

665 *coli* BL21(DE3) LOBSTR cells (Kerafast) to generate the various NEC oligomeric and

666 heterodimeric interface mutants (listed in **Supplementary Table S18**). The expression and

667 purification of NEC220 and some oligomeric interface mutants (NEC-DN$_{UL34}$, NEC-

668 DN$_{UL34}$/SUP$_{UL31}$, NEC-SUP$_{UL31}$, NEC-E37A$_{UL34}$, NEC-T123Q$_{UL34}$, NEC-F252Y$_{UL31}$, and NEC-

669 E153R$_{UL31}$) were described previously [17,22]. The expression and purification of oligomeric

670 interface mutants (NEC-SUP$_{UL31}$/F252Y$_{UL31}$, NEC-SUP$_{UL31}$/E153R$_{UL31}$, and NEC-

671 SUP$_{UL31}$/T123Q$_{UL34}$) and heterodimeric interface mutants (NEC-K137A$_{UL34}$, NEC-R139A$_{UL34}$,

672 NEC-K137A$_{UL34}$/R139A$_{UL34}$, NEC-K137A$_{UL34}$/SUP$_{UL31}$ and NEC-

673 K137A$_{UL34}$/R139A$_{UL34}$/SUP$_{UL31}$) are described below. Cells expressing the corresponding NEC

674 construct were expressed using auto-induction at 37 °C in TB supplemented with 100 μg/mL

675 ampicillin, 100 μg/mL kanamycin, and 34 μg/mL chloramphenicol, 0.2% lactose, and 2 mM

676 MgSO$_4$ for 4 h. The temperature was reduced to 25 °C for 16 h. Cells were harvested at 5,000 x g

677 for 30 min.

678 All purification steps were performed at 4 °C, as previously described [17,28]. Cell pellets

679 were resuspended in lysis buffer (50 mM Na HEPES pH 7.5, 500 mM NaCl, 1 mM TCEP, and

680 10% glycerol) supplemented with Complete protease inhibitor (Roche) and lysed using a

681 microfluidizer (Microfluidics). The cell lysate was clarified by centrifugation at 18,000 x g for

682 40 min and passed over a Ni Sepharose 6 column (Cytiva) equilibrated with lysis buffer. The

683 protein-bound column was washed with 20 mM and 40 mM imidazole lysis buffer and bound

684 proteins were eluted with 250 mM imidazole lysis buffer. Eluted proteins were passed over a

685 Glutathione Sepharose 4B column and washed with lysis buffer. The His$_6$-SUMO and GST tags

686 were cleaved for 16 h by PreScission Protease, produced in-house from a GST-PreScission

687 fusion expression plasmid (a gift of Peter Cherepanov, Francis Crick Institute). The protein was

688 passed over 2 x 1 mL HiTrap Talon columns (Cytiva) to remove His$_6$-SUMO, followed by

689 injection onto a size-exclusion column (Superdex 75 10/300; Cytiva) equilibrated into gel-

690 filtration buffer (20 mM Na HEPES, pH 7.0, 100 mM NaCl, and 1 mM TCEP), as previously

691   described. Fractions containing pure protein, as assessed by 12% SDS-PAGE and Coomassie

692   staining were pooled and concentrated as described below.

693   For both NEC-SUP$_{UL31}$ and NEC-DN$_{UL34}$/SUP$_{UL31}$, the cleaved proteins were passed over

694   a HiTrap SP XL (5 mL; Cytiva) ion-exchange column, to remove free His$_6$-SUMO. Bound

695   proteins were eluted using a linear salt gradient (60 mL) made from no salt gel filtration buffer

696   (20 mM Na HEPES, pH 7.0, and 1 mM TCEP) and salt gel filtration buffer (20 mM Na HEPES,

697   pH 7.0, 1 M NaCl, and 1 mM TCEP). Proteins typically eluted ~ 360 mM NaCl, at which point

698   the gradient was held constant until the UV signal returned to baseline. Fractions containing pure

699   protein, as assessed by 12% SDS-PAGE and Coomassie staining, were pooled and diluted using

700   no salt gel filtration buffer to reach a 100 mM NaCl concentration, which is required for

701   downstream liposome budding experiments described below. For all purifications described

702   herein, the protein was concentrated to ~ 1 mg/mL and stored at -80 °C to prevent degradation

703   observed at 4 °C. Protein concentrations were determined by the absorbance at 280 nm. A typical

704   yield was ~0.5 mg/L.

705

706   ***Expression and purification of membrane interface constructs.*** Plasmids containing UL31 1-

707   306 (pKH90) and UL34 1-220-His$_8$ (pJB57) were co-transformed into *E. coli* BL21(DE3)

708   LoBSTr cells (Kerafast) to generate NEC220-His$_8$. All the following constructs contained UL31

709   1-306 and UL34 1-220 amino acid boundaries. A list of plasmids co-transformed to create the

710   NEC-SE6$_{UL31}$-His$_8$, NEC-SUP$_{UL31}$-His$_8$, and NEC-SE6$_{UL31}$/SUP$_{UL31}$-His$_8$ constructs are listed in

711   **Supplementary Table 18**. Cells expressing the corresponding NEC mutant were grown using

712   auto-induction at 37 °C in TB supplemented with 100 μg/mL ampicillin, 100 μg/mL kanamycin,

713   and 34 μg/mL chloramphenicol, 0.2% lactose, and 2 mM MgSO$_4$ for 4 h. The temperature was

714   reduced to 25 °C for 16 h. Cells were harvested at 5,000 x g for 30 min.

715   Cells were resuspended in lysis buffer supplemented with Complete protease inhibitor

716   (Roche) and lysed using a microfluidizer (Microfluidizer). The cell lysate was clarified by

717   centrifugation at 18,000 x g for 40 min and passed over a Ni Sepharose 6 column (Cytiva). The

718   column was washed with 20 mM and 40 mM imidazole lysis buffer and bound proteins were

719   eluted with 250 mM imidazole lysis buffer. Eluted proteins were passed over a Glutathione

720   Sepharose 4B column and washed with lysis buffer. The His$_6$-SUMO and GST tags were cleaved

721   for 16 h by PreScission Protease, produced in-house from a GST-PreScission fusion expression

722 plasmid. The protein was loaded on a size-exclusion column (Superdex 75 10/300; Cytiva)

723 equilibrated with a gel-filtration buffer. Fractions containing pure protein, as assessed by 12%

724 SDS-PAGE and Coomassie staining were pooled and concentrated as described above.

725

726 ***Expression and purification of crystallization constructs.*** SUP$_{UL31}$Δ50-306 (pXG20) and UL34

727 15-185 (pJB04) or SUP$_{UL31}$Δ50-306 (pXG20) and UL34 15-185 D35A$_{UL34}$/E37A$_{UL34}$ (pJB66)

728 plasmids were co-transformed into *E. coli* BL21(DE3) LoBSTr cells (Kerafast) to produce the

729 NEC-SUP$_{UL31}$ and NEC-DN$_{UL34}$/SUP$_{UL31}$ crystallization constructs, respectively. Cells

730 expressing the corresponding NEC mutant were grown using auto-induction at 37 °C in TB

731 supplemented with 100 µg/mL ampicillin, 100 µg/mL kanamycin, and 34 µg/mL

732 chloramphenicol, 0.2% lactose, and 2 mM MgSO$_4$ for 4 h. The temperature was reduced to 25 °C

733 for 16 h. Cells were harvested at 5,000 x g for 30 min.

734 Cells were resuspended in lysis buffer supplemented with Complete protease inhibitor

735 (Roche) and lysed using a microfluidizer (Microfluidizer). The cell lysate was clarified by

736 centrifugation at 18,000 x g for 40 min and passed over a Ni Sepharose 6 column (Cytiva). The

737 column was washed with 20 mM and 40 mM imidazole lysis buffer and bound proteins were

738 eluted with 250 mM imidazole lysis buffer. Eluted proteins were passed over a Glutathione

739 Sepharose 4B column and washed with lysis buffer. The His$_6$-SUMO and GST tags were cleaved

740 for 16 h by PreScission Protease, produced in-house from a GST-PreScission fusion expression

741 plasmid. The protein was passed over 2 x 1 mL HiTrap Talon columns (Cytiva) to remove His$_6$-

742 SUMO, followed by injection onto a size-exclusion column (Superdex 75 10/300; Cytiva)

743 equilibrated into gel-filtration buffer, as previously described. Fractions containing pure protein,

744 as assessed by 12% SDS-PAGE and Coomassie staining were pooled and concentrated as

745 described above.

746

747 ***In-vitro budding assays.*** Giant unilamellar vesicles (GUVs) were prepared as previously

748 described [17]. For budding quantification, 10 µL of POPC:POPA:POPS=3:1:1 (Avanti Polar

749 Lipids) GUVs containing 0.2% ATTO-594 DOPE (ATTO-TEC GmbH) fluorescent dye were

750 added to gel filtration buffer containing 0.2 mg/mL (final concentration) Cascade Blue

751 Hydrazide (ThermoFisher Scientific) and either 1 µM WT NEC or NEC mutant (final

752 concentration), for a total sample volume of 100 µL. Reactions incubated for 5 min at 20 °C

before imaging in 96-well chambered coverglass (Brooks Life Science Systems). Samples were imaged using a Nikon A1R Confocal Microscope with a 60x oil immersion lens at the Imaging and Cell Analysis Core Facility at Tufts University School of Medicine. Budding events were quantified by manually counting ~300 vesicles total in 15 different frames of the sample. Before analysis, the background (GUVs in the absence of NEC) was subtracted from the raw values. All data values are reported in the **Source Data File**. Each sample was tested in at least three biological replicates, each containing three technical replicates. Reported values represent the average budding activity relative to NEC220 or NEC220-His$_8$ (100%). The standard error of the mean is reported for each measurement. Significance was calculated using an unpaired one-tailed *t*-test against NEC220. Statistical analyses and data presentation were performed using GraphPad Prism 9.1.0.

Complementation assays. 24-well cultures of Hep-2 cells at 70% confluence were transfected with 0.05 μg of pCMVβ, expressing the β-galactosidase gene, and 0.25 μg of wild-type or mutant UL34 plasmid using Lipofectamine as described by the manufacturer (Gibco-BRL) and incubated at 37°C overnight. The cells were then infected with 10 PFU of the BAC-derived UL34-null virus or UL34-null/SUP$_{UL31}$ virus per cell and incubated at 37°C for 90 min. Monolayers were washed once with pH 3 sodium citrate buffer (50 mM sodium citrate, 4 mM potassium chloride, adjusted to pH 3 with hydrochloric acid) and then incubated at room temperature in fresh citrate buffer for one minute. Cells were washed with V medium (Dulbecco's modified Eagle's medium, penicillin-streptomycin, 1% heat-inactivated calf serum) two times. One milliliter of V medium was then added to each well, and after 16 h of incubation at 37 °C, cell lysates were prepared by freezing and thawing followed by sonication for 20 s at power level 2 with a Fisher sonic dismembrator. The amount of infectivity in each lysate was determined by plaque assay titration on UL34-complementing cells. Part of each cell lysate was assayed for β-galactosidase expression as previously described [26]. Transfection efficiencies in all samples were within 20% of each other. Each sample was tested in at least three biological replicates, each containing one technical replicate. The raw titers and log PFU values for each biological replicate are reported in the **Source Data File**.

783 ***Evaluation of mutant protein expression in mammalian cells.*** 12-well cultures of Hep-2 cells at

784 70% confluence were transfected with 0.5 μg of wild-type or mutant UL34 or UL31-FLAG

785 plasmid using Lipofectamine as described by the manufacturer (Gibco-BRL) and incubated at 37

786 °C overnight. The cells were then infected with 10 PFU of the corresponding null virus and

787 incubated at 37 °C for 90 min. The inoculum was then removed and replaced with 1.5 ml V

788 medium, and cultures were incubated for a further 16 hours. Infected cells were harvested by

789 removing the medium, washing the monolayers once with phosphate-buffered saline (PBS),

790 scraping the cells into 1 ml PBS and pelleting the cells at 3,000 rpm in the microcentrifuge for 3

791 minutes. The supernatant liquid was removed, and cell lysates were prepared by resuspending

792 the cell pellets in 25 μl water, adding 25 μl of 2X SDS-polyacrylamide gel sample buffer, and

793 then incubating in a boiling water bath for 10 minutes. Proteins were separated by SDS-PAGE,

794 blotted to nitrocellulose, and then probed with chicken antibody to UL34 (diluted 1:250) [9],

795 mouse antibody to HSV-1 VP5 (diluted 1:500 (Biodesign International) mouse antibody to

796 FLAG epitope (diluted 1:1000) (monoclonal M2, SIGMA/Aldrich) or rabbit antibody to calnexin

797 (diluted 1:1000) (Cell Signaling Technology).

798

799 ***Crystallization and data collection.*** Crystals of NEC185-Δ50-SUP$_{UL31}$ were grown by vapor

800 diffusion at 25 °C in hanging drops with 1 μL of protein (3 mg/mL), 1 μL of reservoir solution

801 (10% PEG3350, 8 mM Li$_2$SO$_4$, 6 mM ATP, and 0.1 M MES, pH 6) and 1 μL of Silver Bullets

802 (Hampton Research) reagent [G3 (0.25% 2,2'-Thiodiglycolic acid, 0.2% Azelaic acid, 0.2%

803 Mellitic acid, 0.2% trans-aconitic acid, 0.02 M HEPES sodium pH 6.8)]. Hexagonal SUP$_{UL31}$

804 crystals appeared after 2 days, only in the presence of Silver Bullets, and were completely grown

805 after one week. Crystals were flash-frozen into liquid nitrogen in a solution identical to the

806 reservoir solution containing 30% glycerol as the cryoprotectant.

807 Crystals of NEC185-Δ50-DN$_{UL34}$/SUP$_{UL31}$ were grown by vapor diffusion at 25 °C in

808 hanging drops with 1 μL of protein (3.5 mg/mL), 1 μL of reservoir solution (10% PEG3350, 14

809 mM Li2SO4, 14 mM ATP, 10 mM phenol, and 0.1 M MES, pH 6) and 1 μL of Silver Bullets

810 (Hampton Research) reagent [G3 (0.25% 2,2'-Thiodiglycolic acid, 0.2% Azelaic acid, 0.2%

811 Mellitic acid, 0.2% trans-aconitic acid, 0.02 M HEPES sodium pH 6.8)]. Hexagonal

812 DN$_{UL34}$/SUP$_{UL31}$ crystals appeared after one week, only in the presence of Silver Bullets.

813 Crystals were flash-frozen into liquid nitrogen in a solution identical to the reservoir solution

814   containing 30% glycerol as the cryoprotectant. In comparison to the SUP_{UL31} crystals,

815   DN_{UL34}/SUP_{UL31} crystals required an additional additive, phenol, and took longer to appear (one

816   week vs. two days).

817

818   ***Cryo-EM grid preparation and image collection.*** A volume of 10 μL of a 1:1 mixture of 400 nm

819   and 800 nm large unilamellar vesicles (LUVs) made of 60% POPC/10% POPS/10% POPA/10%

820   POPE/5% cholesterol/5% Ni-DGS [prepared as previously described [17]] were mixed at room

821   temperature with $NEC220-SE6_{UL31}-His_8$ to a final protein concentration of 1 mg/mL. After 15

822   min incubation, 3 μL of the sample was applied to glow-discharged (45 s) Quantifoil (2/2;

823   Electron Microscopy Sciences) grids. Grids were blotted on both sides for 6 s with 0 blotting

824   force and vitrified immediately by plunge freezing into liquid nitrogen-cooled liquid ethane

825   (Vitrobot), before storage in liquid nitrogen. Grids were loaded into a Tecnai F20 transmission

826   electron microscope (FEI) with a FEG and Compustage, equipped with a Gatan Oneview CMOS

827   camera, using a cryo holder (Gatan) (Brandeis University Electron Microscope Facility). The

828   microscope was operated in low-dose mode at 200 keV with SerialEM. Images were recorded at

829   19,000-fold (pixel size: 5.6 nm) magnification at a defocus of -4 μm. Images are displayed using

830   ImageJ [40].

831

832   ***Cryo-ET grid preparation.*** A volume of 10 μL of a 1:1 mixture of 400 nm and 800 nm large

833   unilamellar vesicles (LUVs) made of POPC:POPS:POPA=3:1:1 [prepared as previously

834   described [17]] was mixed on ice with either WT-NEC220, $NEC-SUP_{UL31}$, or NEC-

835   DN_{UL34}/SUP_{UL31}, each to a final protein concentration of 1 mg/mL. After 30 min incubation, the

836   sample was mixed with 5 nm fiducial gold beads, and cryo-ET grids were prepared by applying

837   3 μL of sample to glow-discharged (30 s) Lacey carbon grids (Electron Microscopy Sciences).

838   Grids were blotted on both sides for 6 s with 0 blotting force and vitrified immediately by plunge

839   freezing into liquid nitrogen-cooled liquid ethane with an FEI Mark IV Vitrobot cryo-sample

840   plunger. Vitrified cryo-ET grids were stored in a liquid nitrogen dewar until use.

841

842   ***Cryo-ET data collection and tomogram reconstruction.*** Tilt series were collected a Titan Krios

843   electron microscope at the California NanoSystems Institute (CNSI). Data collection parameters

844   are listed in **Supplementary Table 11**. Tilt series were collected using SerialEM [41] in a Titan

845   Krios instrument equipped with a Gatan imaging filter (GIF) and a post-GIF K3 direct electron

846   detector in electron-counting mode. Frames in each movie of the raw tilt series were aligned,

847   drift-corrected, and averaged with Motioncor2 [41]. The tilt series micrographs were aligned and

848   reconstructed into 3D tomograms using the IMOD software package [42], then missing-wedge

849   corrected by IsoNet [43] for particle picking.

850

851   ***Sub-tomographic averaging.*** The variation in curvature of the NEC hexagonal coat made it

852   difficult to identify the hexagonal repeat units required for particle picking. To overcome this,

853   particle picking was performed using Python scripts derived from the Particle Estimation for

854   Electron Tomography (PEET) software [44]. Firstly, an initial model was generated as previously

855   described [45] by manually picking ~100 particles and performing sub-tomogram averaging using

856   PEET. This allowed for the hexagonal geometric parameter, including the repeating distance and

857   orients, of the NEC lattice to be accurately measured. Secondly, for each tomogram, a small set

858   of particles were manually picked as "seed" particles sparsely covering all areas containing NEC.

859   The "seed" particle set was then expanded by adding unknown particles near each of the known

860   particles based on the hexagonal geometry obtained above. PEET alignment was performed on

861   the expanded particles to match local conformational changes. Finally, the particle set expansion

862   and PEET alignment were performed iteratively to obtain a complete particle set. Particles with

863   less than three neighbors were excluded from the final particle set to remove outliers.

864   Coordinates and orientations of the final particle set were formatted and imported into Relion [46]

865   for further processing. One round of 3D refinement under bin4 pixel size and several rounds of

866   3D refinement and classification under bin2 pixel size, along with duplicate removal, resulted in

867   the final masked resolutions: WT NEC (5.9 Å), NEC-DN$_{UL34}$/SUP$_{UL31}$ (5.4 Å), and NEC-

868   SUP$_{UL31}$ (13.1 Å). The resolutions reported above for the averaged structures are based on the

869   'gold standard' refinement procedures and the 0.143 Fourier shell correlation (FSC) criterion

870   **(Fig. S5).**

871

872   ***3D Visualization.*** UCSF ChimeraX [47] was used to visualize the resulting sub-tomogram

873   averages in their three dimensions, segmentation of density maps, and surface rendering for the

874   different components of NEC.

875

32

876   ***Data availability.*** All data generated or analyzed during this study are included in the manuscript

877   and supporting files. A source data file is provided for data presented in Figs. 1-4. The cryo-ET

878   sub-tomogram average maps have been deposited in the EM Data Bank under the accession

879   codes EMD-40223 (WT NEC), EMD-40224 (NEC-DN$_{UL34}$/SUP$_{UL31}$), and EMD-40225 (NEC-

880   SUP$_{UL31}$). Atomic coordinates and structure factors for the NEC-SUP$_{UL31}$ crystal structure have

881   been deposited in the RCSB Protein Data Bank under accession code 8G6D. All files will be

882   made publicly available upon publication.

883
884   **References**
885

886   1   Draganova, E. B., Thorsen, M. K. & Heldwein, E. E. Nuclear Egress. *Curr. Issues Mol.*
887   *Biol.* **41**, 125-170, doi:10.21775/cimb.041.125 (2020).

888   2   Roller, R. J. & Baines, J. D. in *Advances in Anatomy, Embryology, and Cell Biology* Vol.
889   223 (ed Klaus Osteirrieder) Ch. 7, 143-169 (Springer, 2017).

890   3   Mettenleiter, T. C., Muller, F., Granzow, H. & Klupp, B. G. The way out: what we know
891   and do not know about herpesvirus nuclear egress. *Cell Microbiol* **15**, 170-178,
892   doi:10.1111/cmi.12044 (2013).

893   4   Reynolds, A. E. *et al.* U(L)31 and U(L)34 proteins of herpes simplex virus type 1 form a
894   complex that accumulates at the nuclear rim and is required for envelopment of
895   nucleocapsids. *J. Virol.* **75**, 8803-8817 (2001).

896   5   Chang, Y. E. & Roizman, B. The product of the UL31 gene of herpes simplex virus 1 is a
897   nuclear phosphoprotein which partitions with the nuclear matrix. *J. Virol.* **67**, 6348-6356
898   (1993).

899   6   Shiba, C. *et al.* The UL34 gene product of herpes simplex virus type 2 is a tail-anchored
900   type II membrane protein that is significant for virus envelopment. *J. Gen. Virol.* **81**,
901   2397-2405 (2000).

902   7   Fuchs, W., Klupp, B. G., Granzow, H., Osterrieder, N. & Mettenleiter, T. C. The
903   interacting UL31 and UL34 gene products of pseudorabies virus are involved in egress
904   from the host-cell nucleus and represent components of primary enveloped but not
905   mature virions. *J. Virol.* **76**, 364-378. (2002).

906   8   Klupp, B. G., Granzow, H. & Mettenleiter, T. C. Primary envelopment of pseudorabies
907   virus at the nuclear membrane requires the UL34 gene product. *J. Virol.* **74**, 10063-10073
908   (2000).

909   9   Roller, R. J., Zhou, Y., Schnetzer, R., Ferguson, J. & DeSalvo, D. Herpes simplex virus
910   type 1 U$_L$34 gene product is required for viral envelopment. *J. Virol.* **74**, 117-129 (2000).

911   10   Bubeck, A. *et al.* Comprehensive mutational analysis of a herpesvirus gene in the viral
912   genome context reveals a region essential for virus replication. *J. Virol.* **78**, 8026-8035,
913   doi:10.1128/JVI.78.15.8026-8035.2004 (2004).

914   11   Lake, C. M. & Hutt-Fletcher, L. M. The Epstein-Barr virus BFRF1 and BFLF2 proteins
915   interact and coexpression alters their cellular localization. *Virology* **320**, 99-106,
916   doi:10.1016/j.virol.2003.11.018 (2004).

917   12   Klupp, B. G. *et al.* Vesicle formation from the nuclear membrane is induced by
918   coexpression of two conserved herpesvirus proteins. *Proc. Natl. Acad. Sci. U. S. A.* **104**,
919   7241-7246, doi:0701757104 [pii]
920   10.1073/pnas.0701757104 (2007).

921   13   Farina, A. *et al.* BFRF1 of Epstein-Barr virus is essential for efficient primary viral
922   envelopment and egress. *J. Virol.* **79**, 3703-3712, doi:10.1128/JVI.79.6.3703-3712.2005
923   (2005).

924   14   Gonnella, R. *et al.* Characterization and intracellular localization of the Epstein-Barr
925   virus protein BFLF2: interactions with BFRF1 and with the nuclear lamina. *J. Virol.* **79**,
926   3713-3727, doi:79/6/3713 [pii]
927   10.1128/JVI.79.6.3713-3727.2005 (2005).

928   15   Desai, P. J., Pryce, E. N., Henson, B. W., Luitweiler, E. M. & Cothran, J. Reconstitution
929   of the Kaposi's sarcoma-associated herpesvirus nuclear egress complex and formation of
930   nuclear membrane vesicles by coexpression of ORF67 and ORF69 gene products. *J.*
931   *Virol.* **86**, 594-598, doi:10.1128/JVI.05988-11 (2012).

932   16   Luitweiler, E. M. *et al.* Interactions of the Kaposi's Sarcoma-Associated Herpesvirus
933   Nuclear Egress Complex: ORF69 Is a Potent Factor for Remodeling Cellular Membranes.
934   *J. Virol.* **87**, 3915-3929, doi:10.1128/JVI.03418-12 (2013).

935   17   Bigalke, J. M., Heuser, T., Nicastro, D. & Heldwein, E. E. Membrane deformation and
936   scission by the HSV-1 nuclear egress complex. *Nat. Commun.* **5**, 4131,
937   doi:10.1038/ncomms5131 (2014).

938   18   Lorenz, M. *et al.* A single herpesvirus protein can mediate vesicle formation in the
939   nuclear envelope. *J. Biol. Chem.* **290**, 6962-6974, doi:10.1074/jbc.M114.627521 (2015).

940   19   Thorsen, M. K., Draganova, E. B. & Heldwein, E. E. The nuclear egress complex of
941   Epstein-Barr virus buds membranes through an oligomerization-driven mechanism. *PLoS*
942   *Pathog.* **18**, e1010623, doi:10.1371/journal.ppat.1010623 (2022).

943   20   Hagen, C. *et al.* Structural basis of vesicle formation at the inner nuclear membrane. *Cell*
944   **163**, 1692-1701, doi:10.1016/j.cell.2015.11.029 (2015).

945   21   Newcomb, W. W. *et al.* The primary enveloped virion of herpes simplex virus 1: Its role
946   in nuclear egress. *mBio* **8**, doi:10.1128/mBio.00825-17 (2017).

947   22   Bigalke, J. M. & Heldwein, E. E. Structural basis of membrane budding by the nuclear
948   egress complex of herpesviruses. *EMBO J.* **34**, 2921-2936,
949   doi:10.15252/embj.201592359 (2015).

950   23   Walzer, S. A. *et al.* Crystal Structure of the Human Cytomegalovirus pUL50-pUL53
951   Core Nuclear Egress Complex Provides Insight into a Unique Assembly Scaffold for
952   Virus-Host Protein Interactions. *J. Biol. Chem.* **290**, 27452-27458,
953   doi:10.1074/jbc.C115.686527 (2015).

954   24   Arii, J. *et al.* Roles of the interhexamer contact site for hexagonal lattice formation of the
955   herpes simplex virus 1 nuclear egress complex in viral primary envelopment and
956   replication. *J. Virol.* **93**, doi:10.1128/jvi.00498-19 (2019).

957   25   Roller, R. J., Bjerke, S. L., Haugo, A. C. & Hanson, S. Analysis of a charge cluster
958   mutation of herpes simplex virus type 1 UL34 and its extragenic suppressor suggests a
959   novel interaction between pUL34 and pUL31 that is necessary for membrane curvature
960   around capsids. *J. Virol.* **84**, 3921-3934, doi:10.1128/jvi.01638-09 (2010).

961   26   Bjerke, S. L. *et al.* Effects of charged cluster mutations on the function of herpes simplex
962   virus type 1 UL34 protein. *J Virol* **77**, 7601-7610 (2003).

963   27   Thorsen, M. K. *et al.* Highly Basic Clusters in the Herpes Simplex Virus 1 Nuclear
964   Egress Complex Drive Membrane Budding by Inducing Lipid Ordering. *mBio* **12**,
965   e0154821, doi:10.1128/mBio.01548-21 (2021).

966   28   Draganova, E. B., Zhang, J., Zhou, Z. H. & Heldwein, E. E. Structural basis for capsid
967   recruitment and coat formation during HSV-1 nuclear egress. *Elife* **9**,
968   doi:10.7554/eLife.56627 (2020).

969   29   Kato, A. *et al.* Identification of proteins phosphorylated directly by the Us3 protein
970   kinase encoded by herpes simplex virus 1. *J. Virol.* **79**, 9325-9331,
971   doi:10.1128/jvi.79.14.9325-9331.2005 (2005).

972   30   Mou, F., Wills, E. & Baines, J. D. Phosphorylation of the U(L)31 protein of herpes
973   simplex virus 1 by the U(S)3-encoded kinase regulates localization of the nuclear
974   envelopment complex and egress of nucleocapsids. *J. Virol.* **83**, 5181-5191,
975   doi:10.1128/jvi.00090-09 (2009).

976   31   Zeev-Ben-Mordehai, T. *et al.* Crystal Structure of the Herpesvirus Nuclear Egress
977   Complex Provides Insights into Inner Nuclear Membrane Remodeling. *Cell Rep.* **13**,
978   2645-2652, doi:10.1016/j.celrep.2015.11.008 (2015).

979   32   Lye, M. F. *et al.* Unexpected features and mechanism of heterodimer formation of a
980   herpesvirus nuclear egress complex. *EMBO J.* **34**, 2937-2952,
981   doi:10.15252/embj.201592651 (2015).

982   33   Krissinel, E. & Henrick, K. Inference of macromolecular assemblies from crystalline
983   state. *J. Mol. Biol.* **372**, 774-797, doi:10.1016/j.jmb.2007.05.022 (2007).

34   Diewald, B., Socher, E., Söldner, C. A. & Sticht, H. Conformational Dynamics of Herpesviral NEC Proteins in Different Oligomerization States. *Int. J. Mol. Sci.* **19**, doi:10.3390/ijms19102908 (2018).

35   Ejercito, P. M., Kieff, E. D. & Roizman, B. Characteristics of herpes simplex virus strains differing in their effect on social behavior of infected cells. *J. Gen. Virol.* **2**, 357-364 (1968).

36   Antinone, S. E., Zaichick, S. V. & Smith, G. A. Resolving the assembly state of herpes simplex virus during axon transport by live-cell imaging. *J. Virol.* **84**, 13019-13030, doi:10.1128/JVI.01296-10 (2010).

37   Tanaka, M., Kagawa, H., Yamanashi, Y., Sata, T. & Kawaguchi, Y. Construction of an excisable bacterial artificial chromosome containing a full-length infectious clone of herpes simplex virus type 1: viruses reconstituted from the clone exhibit wild-type properties in vitro and in vivo. *J. Virol.* **77**, 1382-1391 (2003).

38   Roller, R. J., Hassman, T. & Haugo-Crooks, A. Cell Culture Evolution of a Herpes Simplex Virus 1 (HSV-1)/Varicella-Zoster Virus (VZV) UL34/ORF24 Chimeric Virus Reveals Novel Functions for HSV Genes in Capsid Nuclear Egress. *J. Virol.* **95**, e0095721, doi:10.1128/JVI.00957-21 (2021).

39   Roller, R. J., Haugo, A. C. & Kopping, N. J. Intragenic and extragenic suppression of a mutation in herpes simplex virus-1 UL34 that affects both nuclear envelope targeting and membrane budding. *J. Virol.* **85**, 11615-11625 (2011).

40   Schneider, C. A., Rasband, W. S. & Eliceiri, K. W. NIH Image to ImageJ: 25 years of image analysis. *Nat. Methods* **9**, 671-675, doi:10.1038/nmeth.2089 (2012).

41   Mastronarde, D. N. Automated electron microscope tomography using robust prediction of specimen movements. *J. Struct. Biol.* **152**, 36-51, doi:10.1016/j.jsb.2005.07.007 (2005).

42   Kremer, J. R., Mastronarde, D. N. & McIntosh, J. R. Computer visualization of three-dimensional image data using IMOD. *J. Struct. Biol.* **116**, 71-76, doi:10.1006/jsbi.1996.0013 (1996).

43   Liu, Y. T. *et al.* Isotropic reconstruction for electron tomography with deep learning. *Nat. Commun.* **13**, 6482, doi:10.1038/s41467-022-33957-8 (2022).

44   Nicastro, D. *et al.* The molecular architecture of axonemes revealed by cryoelectron tomography. *Science* **313**, 944-948 (2006).

45   Imhof, S. *et al.* Cryo electron tomography with volta phase plate reveals novel structural foundations of the 96-nm axonemal repeat in the pathogen Trypanosoma brucei. *Elife* **8**, doi:10.7554/eLife.52058 (2019).

1019   46   Scheres, S. H. RELION: implementation of a Bayesian approach to cryo-EM structure
1020   determination. *Journal of Structural Biology* **180**, 519-530, doi:10.1016/j.jsb.2012.09.006
1021   (2012).

1022   47   Goddard, T. D. *et al.* UCSF ChimeraX: Meeting modern challenges in visualization and
1023   analysis. *Protein Sci* **27**, 14-25, doi:10.1002/pro.3235 (2018).

1024   48   Morin, A. *et al.* Collaboration gets the most out of software. *Elife* **2**, e01456,
1025   doi:10.7554/eLife.01456 (2013).
1026